2022 Design of a Human-Powered Vehicle with Electric Assist

The Turbo Trike

Written by:

Hoang Pham (Hoang_Pham2@student.uml.edu)

Michael Mears (Michael_mears@student.uml.edu)

Steven Beaupre (Steven_Beaupre@student.uml.edu)

Derek Chigas (Derek_Chigas@student.uml.edu)

SUBMITTED AS PART OF THE CAPSTONE PROJECT

DEPARTMENT OF MECHANICAL ENGINEERING

COLLEGE OF ENGINEERING

UNIVERSITY OF MASSACHUSETTS LOWELL

05-02-2022

Signatures of Authors: Hoang Pham, Michael Mears, Steven Beaupre, Derek Chigas

Capstone Advisor: Abouhamed Saberi

Professor, Department of Mechanical Engineering

1. Abstract:

Electric bikes for recreation and transportation are becoming more and more popular in the United States. Currently, cars dominate the transportation sector but with an increase in demand to travel on renewable resources, the electric transportation space has grown rapidly. With the creation of The Turbo Trike, the University of Massachusetts Human-powered vehicle team has conceived an environment-friendly alternative that can be used for recreation or transportation. By prioritizing safety, durability, and user-friendliness. The Turbo Trike can help cut down on the use of oil and rely more on leg power with some electric assistance.

A three-wheel delta configuration recumbent vehicle was selected to provide the ideal level of stability, speed, and ease of use. The recumbent tricycle allows back support, reduces stress on the human body, and requires less effort to reach the same speeds as the standard upright bicycle. The design is adjustable and simple so it can be widely used as a mode of transportation or recreation.

The vehicle's relaxed position provides an excellent amount of safety and can give the rider confidence when they are in the Turbo Trike. The steering geometry is designed to prevent rollover and give the rider an excellent amount of control to navigate wherever they need.

The team utilized computer simulation software such as SolidWorks throughout the design process to analyze the structural, aerodynamic, and handling integrity. In the manufacturing phase, the team built the sturdy frame of the model to ensure that the design is strong and safe. The use of MATLAB provided the ability to create programs to determine the speed of the vehicle depending on force input into the pedals. Testing results were used to analyze the vehicle and assure that the vehicle could compete in a competition.

2. Acknowledgment:

The team wishes to acknowledge the guidance of professor Saberi with the design and roadmap for the project. Additionally, the team would also like to express appreciation to the MakerSpace crew at the University of Massachusetts Lowell that helped manufacture the prototype of the product.

3. Table of Contents

List of Figures:

List of Tables:

4. Introduction:

Background and Motivation:

The demand for electric vehicles and environmentally friendly transportation options has increased dramatically in the last ten years. Bicycles, scooters, and roller blades are all friendly ways of transportation but sometimes are not fast enough or require too much effort to go the speed desired. That is why the team here has designed a recumbent tricycle that is fast, reliable, and comfortable. Tricycles have been around since the 1700s and they have only improved from there. The recumbent tricycle known today has many different configurations and designs. The delta design with one wheel in the front and two in the back has been widely used and has been improved upon for generations. The team wanted to design a recumbent tricycle that has the capability of going fast, being safe, and being user-friendly. The Turbo Trike can reach high speeds with minimal effort thanks to the electric-assist and the relaxed aerodynamic position. The electric assist component gives this human-powered vehicle the ability to reach higher speeds which makes it more practical for daily transportation use. The recumbent design allows it to be comfortable, aerodynamic, and efficient.

Through the application of engineering design principles, the development of a sustainable and practical transportation alternative was fabricated. From everyday recreational use to commuting to work, this vehicle can do it all and exemplifies the qualities of safety, sustainability, user-friendliness, and speed. The Turbo Trike remains a practical solution for real-world scenarios where transportation is needed.

Literature Review:

i) The stress analysis used for the frame design was based on the topics of the course MECH.4250: Design of Machine Elements and *Shigley's Mechanical Engineering Design* of R. Budynas, K. Nisbett.

ii) The FEA analysis conducted was studied in the course MECH.3110: Applied Strength of Materials.

iii) The steering system design was based on the linkage analysis from MECH.3210: Kinematics of Mechanism and the “Multitrack Vehicle Handling Performance” section from C. Mark Archibald, *Design of Human-Powered Vehicles.*

iv) The powertrain analysis was based on the gear analysis from MECH.3210: Kinematics of Mechanism.

v) The brake analysis was based on the dynamic analysis of a vehicle taught in ENGN.2070: Dynamics.

5. Project Logistics:

The leadership structure of the team was shared but throughout the semester a leader evolved and gave tasks to the other team members to make sure all aspects of the project are completed on time. The team communicated on discord and worked together after the weekly meeting with the professor who was overseeing the project. The structure of the team was loose as all worked together to help each other with many different parts of the tricycle. The team promoted an inclusive environment by keeping everyone involved and distributing work evenly. Throughout the project, all members remained supportive while still giving honest feedback during brainstorming sessions. The collaborative atmosphere was created by the excitement to achieve the best with this project. From the start of the project, the team was committed to communicating effectively and working together. The atmosphere created made the team more efficient and enjoyable to work with.

The project schedule was set in the beginning but had a lot of changes as time went on. At the beginning, the focus was on the frame of the design. The frame was the priority to design so other parts can be designed around it. After the frame was designed, members of the team started working on the brakes and the steering mechanism. Scheduling to get certain aspects done by the end of the week led to an efficient system where every week produced a lot of progress. Following the schedule, the seat and wheels had to be added to the SolidWorks file. According to the schedule, the plan was to test the model during the last week to determine its crash safety, the rollover bar, turning radius, and many other factors. The team was held accountable to the schedule by each other and by the professor. The team was given guidance on what to focus on each week, and this helped the team focus on what is most important.

Safety is a major point of consideration when in the designing phase. The focus was on the structural integrity of the frame and safety accessories. The requirements on safety were a top priority and included brakes, rollover possibility, harness, and much more. The crash safety had to be tested to see if the frame geometry is strong enough. To ensure a rollover wasn't easy to occur a lot of extra consideration had to go into the steering system. This ensures that at higher speeds and turning, rollovers do not occur.

6. Design Methodology:

Approaching the design process, the layout for the vehicle was first decided. The mission of the American Society of Mechanical Engineers' (ASME) Human Powered Vehicle Competition (HPVC) is to provide "…an opportunity for students to demonstrate the application of sound engineering design principles in the development of sustainable and practical transportation alternatives… to design and build efficient, highly engineered vehicles for everyday use-from commuting to work, to carrying goods to market." For this reason, the team at UMass Lowell sought to bring these ideals to life in the engineering of the vehicle. The goal was to design a recumbent tricycle that exemplifies the qualities of safety, sustainability, speed, and user-friendliness. The project was based on the requirements and restraints of the ASME recumbent bike competition. These rules and constraints gave a guideline of what can be done and what is expected. Identifying opportunities by having brainstorming sessions gave the team the ability to

innovate and design something different from an average recumbent trike while still having the trike remain practical for real-world scenarios.

The team initially thought of a recumbent bike due to its advantages of speed and comfort for users. Looking into quad, tricycle, and bicycle designs the team decided that a tricycle design was the best for stability, speed, and ease of use at low speeds.

Design Flow Chart:

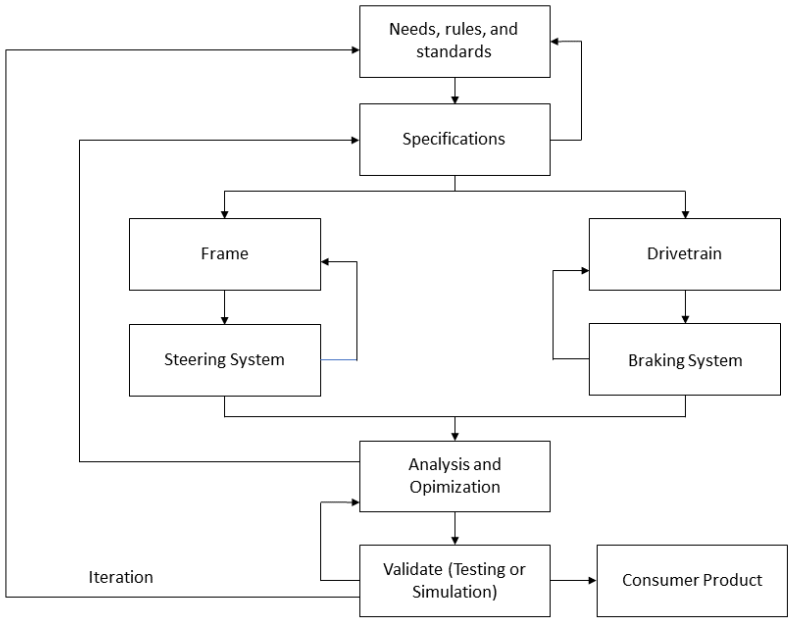

Figure 6.1: Design chart for the human power vehicle challenge with electric assist

Specifications and Requirements:

To help facilitate the design process one of the first steps was creating a specifications and requirements chart. The requirements described in Table 6.1 is what the vehicle was designed around.

Table 6.1: Human Powered Vehicle Specifications and Goals

Specifications	Requirements
Turn Radius	• ≥ 8 m (26.2 ft)
Braking	• Comes to a stop from 25 km/h (22.78 ft/s) in a distance of 6.0 m (19.7 ft) • Properly designed brakes for front wheels • If there are multiple front wheels, brakes are required for each

Speed	• Max: 20 mph with throttle assistance • Stably travel for 30 m (98.4 ft) in a straight line at a speed of 5 to 8 km/h (4.56 – 7.3 ft/s)
Safety Harness	• Safety harnesses with lap and shoulder belts • Commercially available harnesses designed for automotive, aviation or racing applications will generally be accepted without test data for the straps and buckles. • Test data for attachment points may still be required at the time of the safety inspection.
Electric components	• Limited to class 1-3 electric bicycle specifications • Limited to low voltage DC 48V • Starting with stored energy is encouraged • **Class 1**: eBikes that are pedal-assist only, with no throttle, and have a maximum assisted speed of 20 mph. • **Class 2**: eBikes that also have a maximum speed of 20 mph, but are throttle-assisted. (Most likely goal) • **Class 3**: eBikes that are pedal-assist only, with no throttle, and a maximum assisted speed of 28 mph. • All classes limit the motor's power to 1 horsepower (750W).

Frame Methodology:

The most important component for a human-powered vehicle is the frame. The steps used to design the frame for the vehicle consists of frame configuration selection, frame material selection, frame dimensioning, stress analysis, and FEA modeling.

Frame configuration selection*:*

Firstly, the frame configuration must be determined in order to begin the layout dimensioning process. A trade-off study was conducted to select between multiple human-powered vehicle configurations on the market: tadpole, delta, delta with tilt steering, and the classic bicycle. Table 6.2 shows the decision matrix used to rank the configurations.

Table 6.2: Decision matrix for the frame configuration

Frame Configuration		**Tadpole**	**Delta**	**Delta-Tilting**	**Bicycle**
Categories	Weight [1-5]	Value [1-10]	Value [1-10]	Value [1-10]	Value [1-10]
Comfort	3	8	9	6	4
Weight	4	7	7	7	9
Maneuverability	3	6	7	5	8
Speed	4	8	9	6	9
Manufacturability	4	8	8	6	8
Total		134	**144**	109	140

As seen in Table 6.2, four parameters were used for the tradeoff study of the configurations: comfort, weight, maneuverability, speed, and manufacturability.

Since the user is expected to use the vehicle for a prolonged period of time, comfort is an important parameter for the vehicle, with a weight of 3. For the tadpole and delta trike configuration, the user will be operating the vehicle in a laid-down position. Therefore, the user will feel less tired even after using the vehicle for a long time. Therefore, the two scored an 8 and 9, respectively. The delta-tilting is similar; however, the user will have to tilt the whole vehicle in order to steer, and this significantly reduces the comfortability of the vehicle, resulting in a score of only 6. For the bicycle, the user will have to either lean forward or sit in an upright position; hence, the configuration only scored a comfort level of 4.

Secondly, the weight of the vehicle was also an important parameter to consider for ease of transfer and user experience while riding. The tadpole, delta, and delta-tilting configurations have similar layouts and components; thus, their weight will be close to each other, so all three scored 7 for this category. On the other hand, the bicycle configuration will weigh less since the frame can be made smaller with fewer components required. Hence, the bicycle configuration scored a 9.

Thirdly, maneuverability was a factor to consider for the configurations. In order to be able to ride the vehicle on road with many turns, the vehicle must be maneuverable. This is the reason why the category weight was 3. The delta-tilting can be difficult to control in these types of road terrain, so it scored a 5. The tadpole and delta perform similarly (with a score of 6 and 7, respectively), with the delta having a small edge due to the easier steering control system. The bicycle configuration only requires the steering of one axis, and it can be controlled easily by turning the handlebar; thus, the configuration scored an 8.

Moving on, the speed also significantly impacts the user experience, with a weight of 4. The delta-tilting configuration is difficult to achieve high speed due to instability issues. As a result, the configuration only scored a 6. On the other hand, the tadpole and delta configuration can reach higher speed since these configurations are more stable, which resulted in a score of 8 and 9, respectively. Similarly, the bicycle configuration can reach high speed due to its lightweight and stability, resulting in a score of 9.

Finally, manufacturability is a critical parameter to minimize production labor and cost. The del-tilting configuration is more difficult to manufacture due to the more complex components required for the tilting mechanism of the vehicle; thus, it only scored a 6. On the other hand, the remaining three configurations have significantly similar components, and they are easier to manufacture compared to the delta-tilting. Consequently, all three scored an 8 for manufacturability.

From the decision matrix, the delta configuration is the most viable layout for the vehicle, with the bicycle configuration coming second. Hence, the delta configuration was chosen for the design of the vehicle.

Frame material selection:

After the layout for the vehicle was chosen. A similar trade-off study was conducted for the material of the frame. Table 6.3 shows the decision matrix used to evaluate different materials for the frame.

Table 6.3: Decision matrix for the frame material

Frame Material		**6061 Aluminum**	**304 Stainless Steel**	**Carbon Fiber**	**7005 Aluminum**
Categories	Weight [1-5]	Value [1-10]	Value [1-10]	Value [1-10]	Value [1-10]
Cost	5	7	9	2	5
Weight	4	9	3	10	8
Strength	3	7	8	9	8
Reusability	2	9	8	4	9
Manufacturability	4	8	8	5	9
Total		**142**	129	105	135

Firstly, in order to produce a vehicle that could be mass-produced and sold in the market, the price for the vehicle must be reasonable, which is highly dependent on the manufacturing cost. Since the majority of the cost of the vehicle lies within the frame, the cost was the most important parameter for selecting frame material. Hence, this parameter had a weight of 5. 304 stainless steel has the lowest cost out of the material, so a score of 9 was given for steel. 6061 aluminum was more expensive than the 304 stainless steel; however, it cost less than 7005 aluminum. Additionally, carbon fiber was significantly more expensive than the other material; as a result, 6061 aluminum, 7005 aluminum, and carbon fiber scored 7, 5, and 2 for the cost criterion, respectively.

Secondly, the weight (density) of the material was pivotal to be able to achieve a lightweight vehicle. Though 304 stainless steel cost the least, it had a significantly higher density compared to other materials, resulting in a score of only 3 for the material. On the contrary, carbon fiber was the lightest material, which scored a 10. 6061 aluminum and 7005 aluminum had similar densities, with 7005 aluminum being heavier, which resulted in a score of 9 and 8, respectively.

Thirdly, the strength of the material was also chosen as an important parameter since the frame has to be able to support the user and resist the road loads. 304 stainless steel and carbon fiber, which scored 8 and 9, respectively, had higher strength compared to the aluminum alloys. 6061 aluminum and 7005 aluminum scored 7 and 8 since they have similar strength properties.

Fourthly, the reusability was also taken into account for the material selection process of the frame. The reusability is an environmental consideration since it revolves around how the material of the frame would be processed at the vehicle's end of life. Materials such as 6061 aluminum, 7005 aluminum, and 304 stainless steel can be recycled and used for other applications. These materials will less likely become unwanted waste and harm the environment. Hence, 6061 aluminum, 7005 aluminum, and 304 stainless steel scored 9, 9, and 8. In contrast, a carbon fiber frame would be hard to recycle, and there is a chance the user may incorrectly dispose of the material, causing environmental damage. As a result, carbon fiber only scored a 4.

Finally, manufacturability must be considered for the frame material selection. This had a weight of 4. With available machining processes (e.g. milling, cutting, drilling, etc.), materials such as 6061 aluminum and 304 stainless steel can readily be machined into the correct geometry for the frame, which is the reason why these materials scored an 8. 7005 aluminum's advantage also includes its weldability; hence, the score of 9. Due to the limited and costly manufacturing processes for carbon fiber, the material was only assigned a 5.

In conclusion, from the decision matrix, 6061 aluminum was decided as the best material for the frame due primarily due to its lightweight, manufacturability, and reasonable cost.

***Frame dimensioning**:*

The initial dimensions for the frame were determined based on similar vehicles with the same configuration. The dimensions are shown in Table 6.4.

Table 6.4: Table of dimensions for similar delta trike vehicles

Model	Wheelbase (inch)	Track (inch)
Trix [11]	46	34
Mobo Triton Pro [12]	48	28
Kettlewiesel All Round [13]	46	34
Trigo [14]	50	32
Kettlewiesel Evo Steps [15]	52	35.5
Average	48.4	32.7

The average values for the wheelbase and track were used as starting point for the dimensioning of the frame. Multiple iterations were tested in order to select the optimal dimensions based on the mounting points and wheel size. Additionally, the dimensions were also tested for stress to ensure no yielding occurred when during usage.

The main parts of the frame were connected through bolts instead of welding for ease of disassembly; hence, the vehicle can be shipped more easily. The stresses in the bolt were also analyzed in shear and in tension in order to ensure the fasteners operate correctly.

Stress Analysis:

With the dimensions of the frame decided, a force analysis was conducted on the frame.

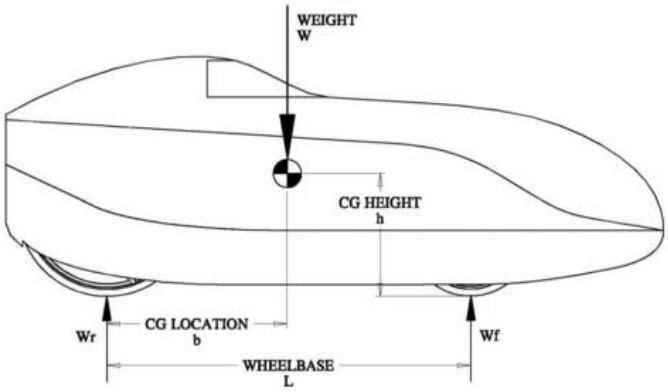

Figure 6.2: Load on static vehicle [1]

Figure 6.2 shows the force on a static vehicle. From the FBD analysis of the vehicle, the vertical load on each axle of the vehicle can be expressed as:

$$W_f = \frac{b}{L}W \tag{6.1}$$

$$W_r = \frac{L-b}{L}W \tag{6.2}$$

where W is the weight of the vehicle, W_f is the vertical load on the front wheel, and W_r is the vertical load on the rear wheels.

The frame was modeled in SolidWorks and the components were assigned the correct materials decided prior. From there, an estimation of the weight and the location of the center of gravity of the vehicle was determined. Additionally, the average weight in the U.S was used for the approximation weight contribution of the user. Therefore, the front wheel weight and the rear wheel weight was readily calculated.

The configurations of the bolts were also analyzed in order to calculate the stresses for the static analysis. [9]

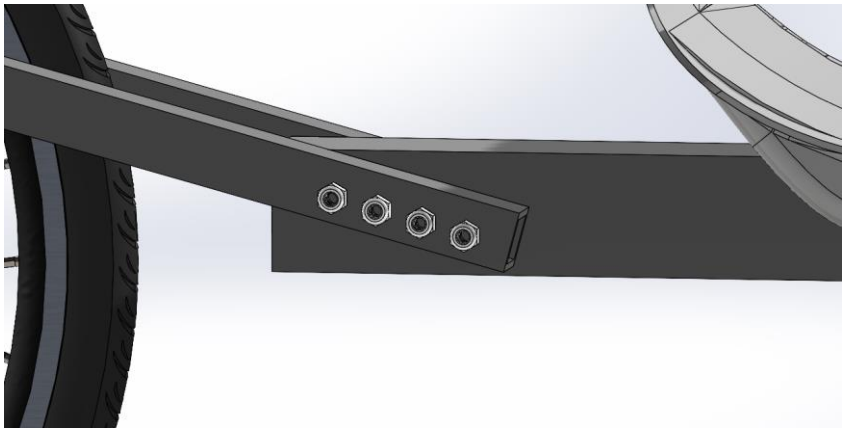

Figure 6.3: Bolts to connect the main frame to the front bars

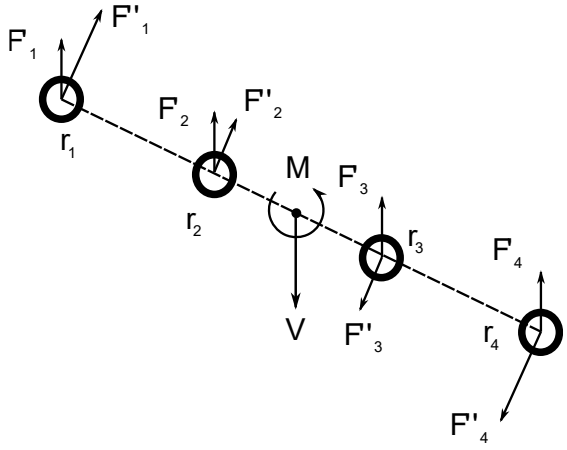

Figure 6.4: FBD of the bolts

As seen in Figure 6.4, the bolts connecting the main frame to the front bars are in shear. As a result, a FBD can be used to analyze forces acting on each bolt [9]. F_i' represents primary shear on the bolts, and it was calculated as:

$$F'_i = \frac{V}{4} \tag{6.3}$$

where V is the shear force acting at the centroid of the bolts.

The secondary shear, F''_i, was calculated as:

$$F_i'' = \frac{Mr_i}{r_1^2 + r_2^2 + r_3^2 + r_4^2} \tag{6.4}$$

The total force acting on the bolt was calculated as a vector sum of the primary and secondary shear force. From there, the shear stress in the bolt was calculated as:

$$\tau_i = \frac{F_i}{A_i} \tag{6.5}$$

where F_i is the resultant force in the bolts.

The factor of safety for the bolts was calculated using:

$$FOS = \frac{\sigma_y}{\tau} \tag{6.6}$$

where σ_y is the yield strength of the material for the bolts.

If the factor of safety is greater than 1, the design was accepted. However, if the factor of safety was lower than 1, the design had to be re-evaluated, and more iterations had to be tested to reach an acceptable design.

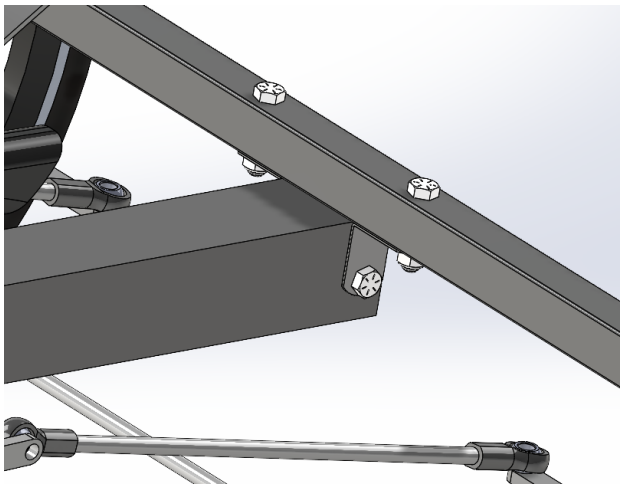

Figure 6.5: Rear bolts

The bolts on the main frame at the rear of the vehicle were also analyzed similarly. However, the bolts on the upper bar were in tension instead of shear. As a result, these bolts were modeled as springs using the equation.

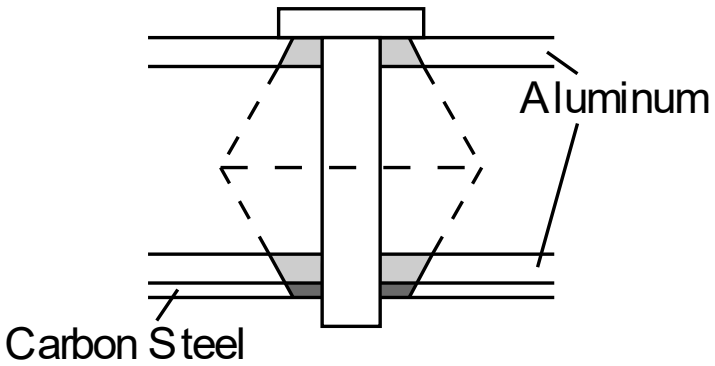

Figure 6.6: Spring model for the fasteners

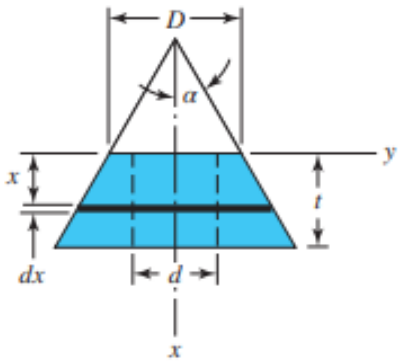

Figure 6.7: Frustum model [9]

Figure 6.7 shows the bolt in tension through the hollow aluminum frame and the carbon steel bracket. The walls of the aluminum bar and the carbon steel brackets were also modeled as springs using the frustum representation in Figure 6.7. The spring constant for these frustums can be expressed as [9]:

$$k = \frac{0.5774\pi Ed}{\ln\frac{(1.155t + D - d)(D + d)}{(1.155t + D + d)(D - d)}} \tag{6.7}$$

where k is the spring constant, E is the Young's modulus of the material, and the remaining parameters are shown in Figure 6.7.

The member springs were considered to be in series; therefore, the member spring constant was calculated using:

$$\frac{1}{k_m} = \frac{1}{k_1} + \frac{1}{k_2} + \frac{1}{k_3} \tag{6.8}$$

Additionally, the spring constant of the bolt can be modeled as:

$$k_b = \frac{A_d A_t E}{A_d l_t + A_t l_d} \tag{6.9}$$

where A_d is the major diameter area, A_t is the threaded cross-section area, l_t is the threaded length, and l_d is the major diameter length.

Therefore, the stiffness constant of the joint was calculated as:

$$C = \frac{k_b}{k_b + k_m} \tag{6.10}$$

With the spring constants known, the force acting on the bolt was easily calculated, and three conditions were tested: factor of safety against proof strength, load factor, and factor of safety against joint separation.

$$n_P = \frac{S_P A_t}{CP + F_i} \tag{6.11}$$

$$n_L = \frac{S_P A_t - F_i}{CP} \tag{6.12}$$

$$n_0 = \frac{F_i}{P(1 - C)} \tag{6.13}$$

where P is the force at the location of the fastener, S_p is the proof strength, and F_i is the preload.

For non-permanent, the preload force is recommended as:

$$F_i = 0.75 A_t S_P \tag{6.14}$$

If the factor of safety calculated was greater than 1, the fasteners were accepted to connect the components of the frame. The calculations were conducted in MATLAB (Appendix C) in order to be able to alter to iterate the dimensions to achieve the desired result.

FEA Modeling:

The analytical calculations shown above require certain assumptions. As a result, FEA modeling was also used in order to calculate and validate the stresses. The FEA modeling was first utilized for the static analysis of different components for the frame.

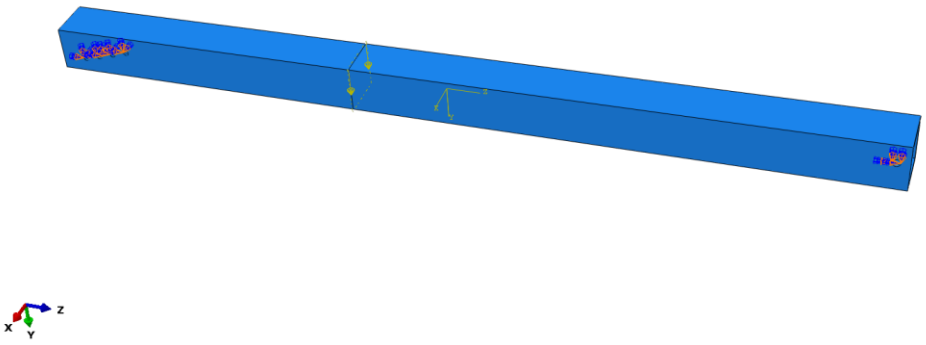

Figure 6.8: Static force and fixed boundary conditions at the holes for the main frame

As seen in Figure 6.8, the load contribution of the user was assumed to be close to the center of mass since the location of the seat can be adjusted to achieve this. As a result, the total weight of the vehicle and the user was applied at the center of mass. Fixed boundary conditions were applied at the mounting holes, where the bolt will be inserted.

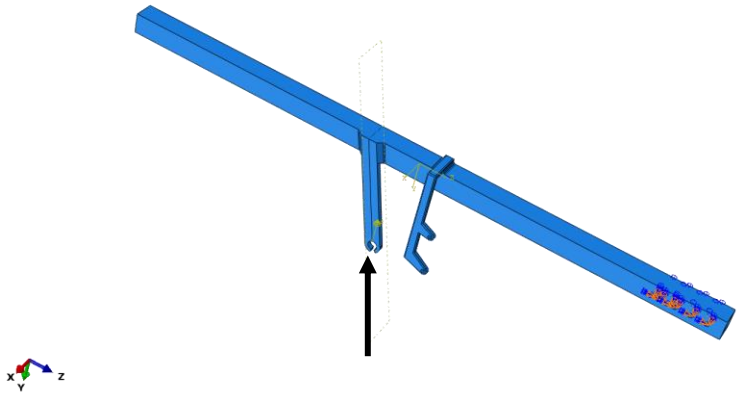

Figure 6.9: Static force and fixed boundary condition at the holes for the front left bar

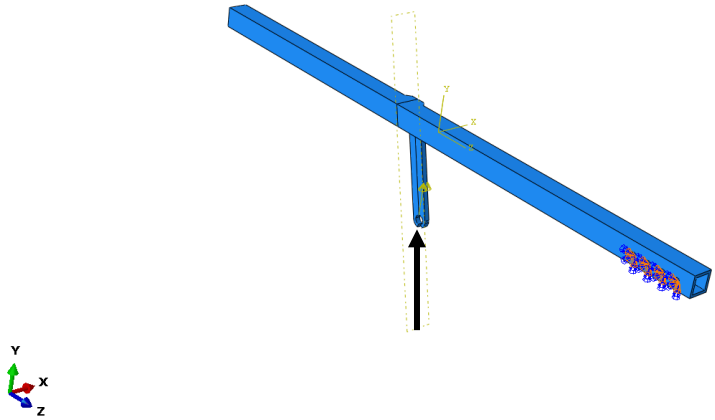

Figure 6.10: Static force and fixed boundary condition at the holes for the front right bar

Figures 6.9 and 6.10 show the FEA modeling for the two front bars. The vertical load applied to each of these bars was assumed the same and equal to half of the front wheel vertical load. The load was applied vertically at the mounting point of the wheel, and the fixed boundary conditions were utilized at the holes where the bolts will be placed.

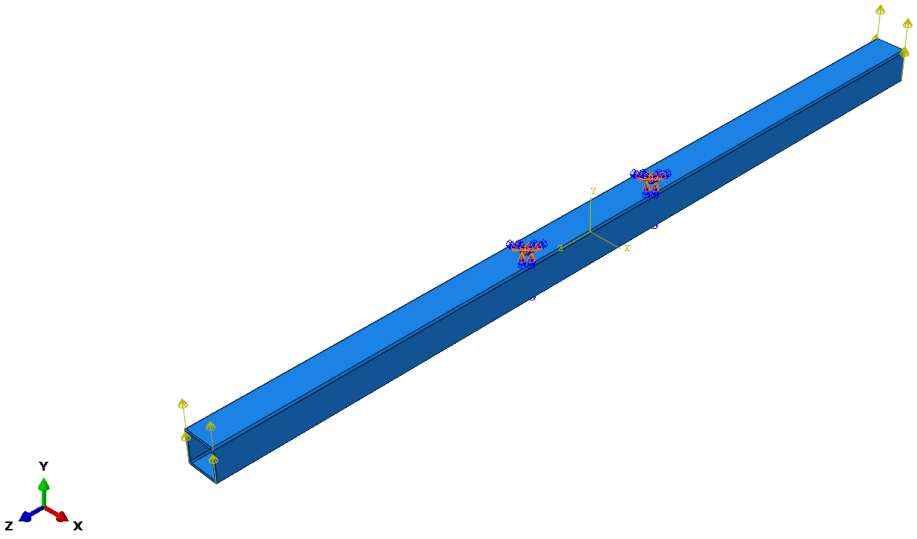

Figure 6.11: Static force and fixed boundary condition at the hole for the rear frame

Figure 6.11 shows the FEA modeling for the rear frame. The vertical rear loads were applied at the sides of the frame. The fixed boundary conditions were applied at the vertical holes where the bolts were located.

From the FEA results, the maximum stress was compared to the yield strength of 6061 aluminum, and the factor of safe was calculated. If the factor of safety is higher than 1, the design was considered appropriate.

The FEA modeling was also utilized to model a low-speed frontal collision. According to the Consumer Product Safety Commission (CPSC), the frame must pass a physical test. However, with the limitation of testing equipment, FEA modeling allowed a simulation of the frame test based on CFR part 16, 1512.14.

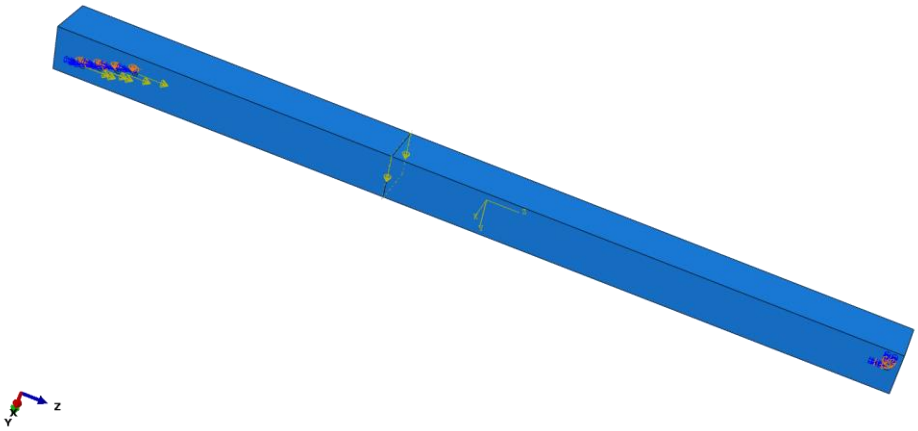

Figure 6.12: Low-speed collision force and fixed boundary condition for the main frame

Figure 6.12 shows the low-speed crash FEA modeling for the main frame. In addition to the vertical load, a load of 200 lb was applied horizontally to the frame. The frame was still fixed at the holes for the bolts.

The remaining components were also applied a similar load. The factor of safety was again analyzed in order to validate that the frame did not yield during a low-speed crash.

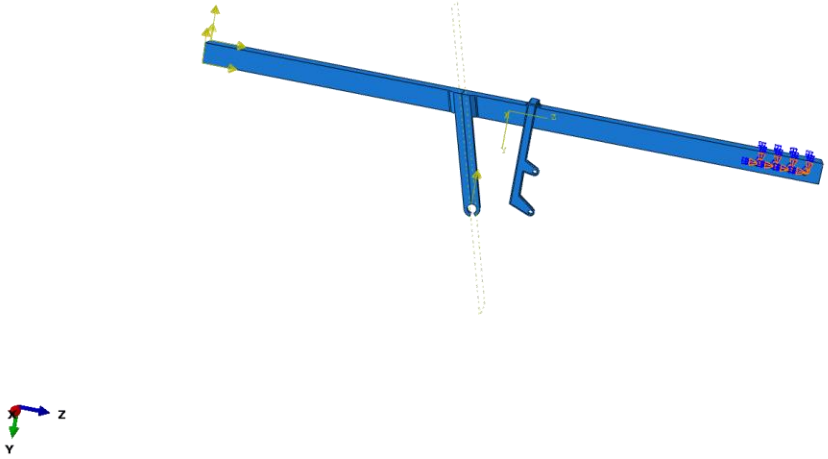

Figure 6.13: Low-speed collision force and fixed boundary condition for the front left bar

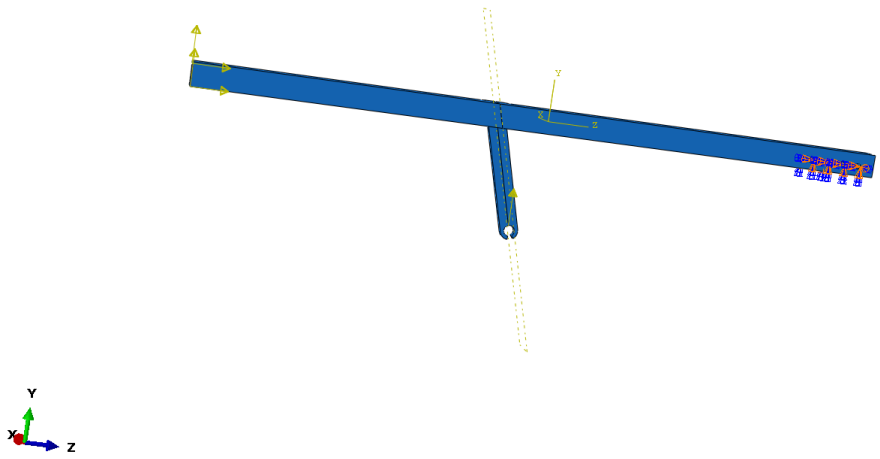

Figure 6.14: Low-speed collision force and fixed boundary condition for the front right bar

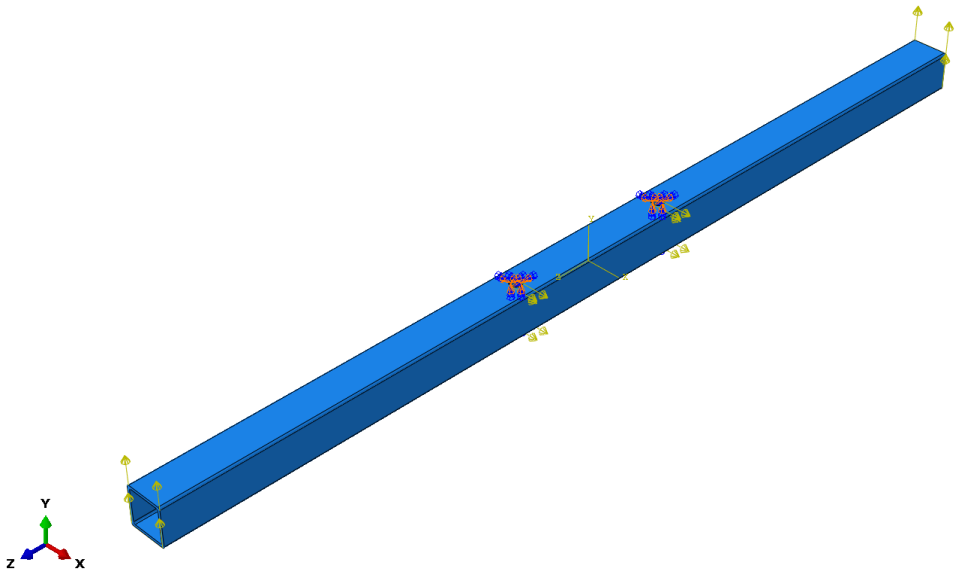

Figure 6.15: Low-speed collision force and fixed boundary condition for the rear frame

Steering system:

Unlike the classic bicycle, the vehicle is considered a multi-track vehicle, which has at least one axle with more than one wheel. A steering analysis must be conducted to avoid significant slip and to provide reliable handling capabilities while turning.

The design process for the steering system started by determining the requirements for the minimum turning radius of the vehicle. This can be found in the ASME Human Powered Vehicle Challenge rule book for 2021 [3]. As a result, the vehicle must be able to turn with a minimum radius of 26.2 ft.

The next step was to select the appropriate steering mechanism best suited for the rear wheels steering of the vehicle. This is followed by the position and sensitivity analysis of the steering system to determine the required dimensions for the steering system. Finally, the detail design step will be conducted to select components and determine how the steering system will be incorporated onto the specific vehicle.

Vehicle Nomenclature:

The steering system of a multi-track vehicle is highly dependent on the dimensions of the vehicle. Therefore, a short description of the nomenclature will be introduced to aid the comprehension of the steering system design process.

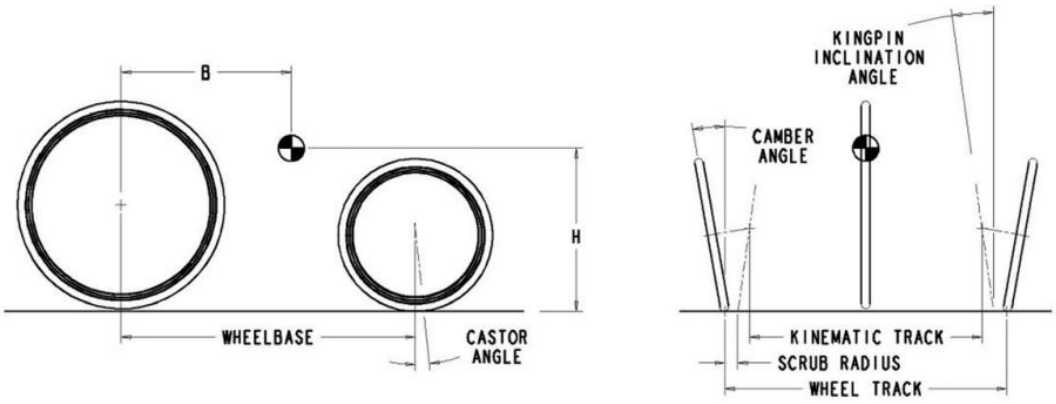

Figure 6.16: Vehicle Nomenclature [1]

In Figure 6.16, the wheelbase is defined as the longitudinal distance from the rear axle to the front axle. “b” refers to the distance from the front axle to the center of gravity, and “h” is the height of the center of gravity above the ground. The kingpin angle is the angle between the steering axis and a vertical plane viewing from the front of the vehicle. The camber angle is the inclination of the wheel from the vertical plane. The wheel track is the horizontal distance between the contact patches of the wheels. The scrub radius is the horizontal distance from the wheel contact patch and the intersection of the steering axis and the ground. Finally, one of the most important parameters in design is the steering system is the kinematic track, which is the horizontal distance between the intersection of the wheel axes and the steering axes.

Steering mechanism selection:

Before determining the dimensioning and analysis step, an appropriate steering mechanism must first be identified for the rear wheel steering goal of the vehicle. Three commonly used steering mechanisms are: Track Rod, Six-Bar Mechanism, and Rack and Pinion (Figure 6.17). These options will be evaluated using a decision matrix to obtain the optimal solution for the rear-wheel steering system.

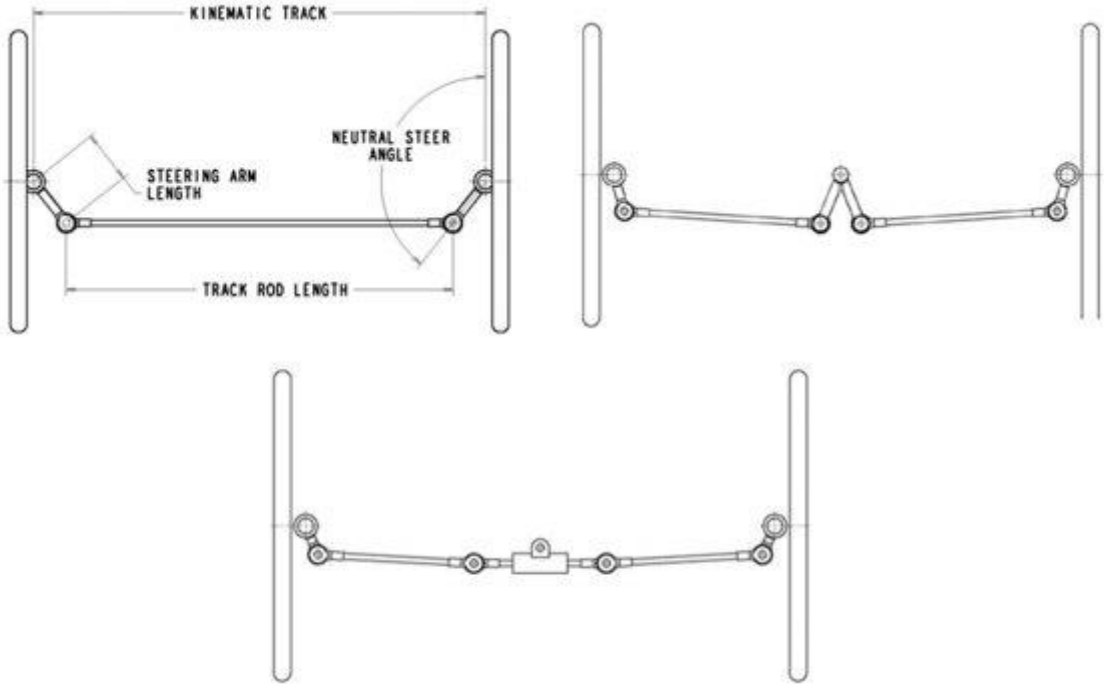

Figure 6.17: Common steering mechanisms: track rod (top left), six-bar (top-right), and rack & pinion (bottom)

Table 6.5: Decision matrix for the steering mechanism

Steering Mechanism		**Track Rod**	**Six-Bar Mechanism**	**Rack & Pinion**
Categories	Weight [1-5]	Value [1-10]	Value [1-10]	Value [1-10]
Accuracy	5	7	9	8
Complexity	3	9	6	7
Sensitivity	2	7	8	9
Manufacturability	4	8	5	4
Total		**108**	99	95

Table 6.5 shows the decision matrix used to pick the optimal steering mechanism for the vehicle. Each parameter is assigned a weight, and each mechanism is scored based on the different parameters. The steering system with the highest weighted sum of the score was selected for the steering system.

As seen in the table, the first parameter considered was the accuracy. This refers to the ability of the steering mechanism to reduce slipping while turning. This main purpose of the steering system, so the accuracy was assigned the highest weight of 5. Since the track rod steering mechanism operates based on the principle of a four-bar linkage, the range of motion, though sufficient, is limited compared to the other options. Hence, it scored only a 7 for this category. On the other hand, the six-bar mechanism has more independent variables (design parameters that can be changed), there will be more range of motion, and hence, higher accuracy can be

achieved, which results in a score of 9 for the six-bar in this category. For the rack and pinion steering system, the rack and pinion controls tie rods connected to the steering axis of the wheel. This results in an accuracy somewhere between the track rod and the six-bar mechanism; thus, the rack and pinion mechanism scored an 8 for accuracy.

The second parameter considered was the complexity of the mechanism. This included the number of components and the challenge for the analysis of the mechanism as a whole. The complexity parameter has a fairly important weight on the design of the steering system given the limited budget and time for the project; therefore, it was given a weight of 3. The track rod scored a 9 in this category since there are only three required components for the mechanism: the track rod and the two steering arms; this also means that the analysis and simulation for the track rod would be less challenging compared to the other two mechanisms. On the other hand, the six-bar mechanism requires six components, and different configurations can also be implemented for the mechanisms. Hence, it only scored a 6 for the parameter. The rack and pinion mechanism requires gears to be selected along with tie rods and steering arms, so it scored a 7 for the category.

The third parameter evaluated was the sensitivity of the mechanism. This category did not necessarily refer to the actual sensitivity of each mechanism because the sensitivity can be changed based on the specific dimensions for the designs. However, this category defines a way to quantify the challenge required to modify the sensitivity of the steering system. Since this parameter was deemed to be more of a consideration rather than requirement, it was assigned a weight of 2. For the track rod mechanism, in order to change the sensitivity, a separate linkage or handlebar must be used. This requires additional components to the main steering system, which can add more failure points for the mechanism. As a result, the track rod scored a 7 for this category. The six-bar mechanism naturally contains a handlebar, so no additional parts will be required to adjust the sensitivity; hence, it scored 8. To change the sensitivity of the rack and pinion mechanism, only the number of teeth on the pinion must be changed. This is an advantage for this steering mechanism, which is the reason why the rack and pinion system scored a 9 for this category.

The final parameter is the manufacturability for the steering system, which includes both the processes that will have to be utilized to make the components and the assembly of the parts. For the track rod, the components are similar to that of a four-bar linkage, which are mainly threaded rods with attached ball-joint rod ends. These components are available from most common vendors, and the assembly process is fairly simple. As a result, the track rod scored an 8 for manufacturability. The six-bar mechanism was similar; however, in addition to requiring more components, it also requires a special shaped linkage for the handlebar pivot. This both complicates the sourcing options and the assembly process, resulting in a score of only 5 for the six-bar mechanism. The rack and pinion required customized gear to be manufactured, and these require precise tolerances. Consequently, this mechanism only scores a 4 for this category.

From the decision matrix, it is clear that the track rod is the best choice for the steering system for the vehicle. The track rod mechanism was selected to be analyzed and used of the dimensioning for the steering system. However, one of the benefits of using the decision matrix

is the flexibility in the design process. If it is determined that the track rod does not satisfy or is difficult to implement due to conflicts with other systems, the second or third option has already been evaluated, and the implementation process can be started immediately without delay. This helps keep the project on track and offers an iterative characteristic to the design process.

Steering system analysis and dimensioning:

When a multi-track vehicle turns, the inside and outer wheels will sweep out different radii. As a result, the inside wheel must have a larger steering angle than the outer wheel. These angles are defined as the Ackerman angles, and they are dependent on the wheelbase, kinematic track, and turning radius. These angles can be calculated as:

$$\delta_i = \tan^{-1}\left(\frac{L}{R - \frac{T}{2}}\right) \tag{6.15}$$

$$\delta_o = \tan^{-1}\left(\frac{L}{R + \frac{T}{2}}\right) \tag{6.16}$$

where L is the wheelbase, T is the kinematic track, and R is the turning radius.

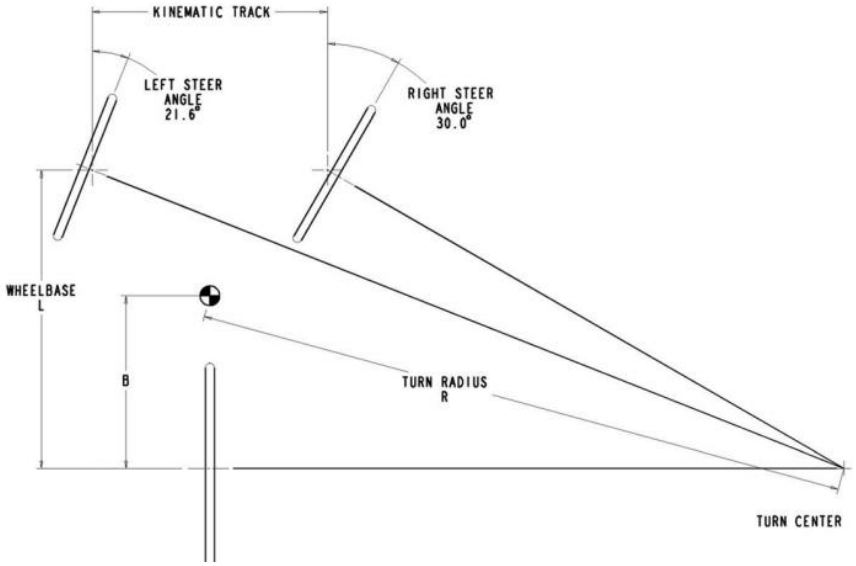

Figure 6.18: Ackerman steering angle [1]

If these angles are achieved, the vehicle will not slip during a turn. However, these are only theoretical values since no steering mechanism can yield the angles exactly. The chosen steering mechanism (track rod) provides good Ackerman compensation. Additionally, the dimensions of the steering mechanism can be optimized to reduce the steering angle error, and if properly designed, the steering error is quite small.

Commonly, for front-wheel steering, the track rod is placed behind the wheel axle to achieve accurate steering angles. However, since the vehicle is designed for rear-wheel steering, the track rod mechanism must be reversed, so the track rod is positioned in front of the rear wheel axle.

As seen in Figure 6.18, with the kinematic track and the wheelbase decided based on previous vehicle requirements, there are only two variables that must be decided for the track rod mechanism: steering arm length and neutral steering angle. A good starting point for the neutral steering [1] can be shown as:

$$\theta_{neutral} = \tan^{-1}\left(\frac{3T}{4L}\right) \tag{6.17}$$

This is determined by drawing a line through the steering arm which intersects the vehicle centerline two-thirds from the rear.

However, this only provides an initial value. In order to optimize the steering mechanism, a MATLAB program was developed to evaluate the design and minimize the steering error.

A track rod steering mechanism in reality is usually non-planar, and the links move in a complex manner in three dimensions. However, the program works based on the assumption that the links of the steering mechanism are all on one plane. This simplifies the analysis; this comes with an accuracy loss. However, the loss of accuracy is usually negligible for practical applications [1].

The MATLAB program was developed using two main parts: position analysis and optimization. As seen in Figure 6.17, the track rod steering mechanism is a four-bar linkage system. As a result, a position analysis can be applied to calculate the resulting steering angles with a certain input.

The dimensions of steering links (steering arms and track rod) are assumed an initial value. From there, if the angle θ_2 was prescribed, the position of all the other links can be calculated. The resulting angle of interest θ_4 can be calculated as [10]:

$$\theta_4 = 2\tan^{-1}\left(\frac{-B - \sqrt{B^2 - 4AC}}{2A}\right) \tag{6.18}$$

A, B, and C are calculated based on the assumed dimensions and input angle θ_2. More details can be found in [10].

If the change of θ_2 with respect to the neutral position of the left steering arm was the prescribed outer Ackerman steering angle, the change of θ_4 will result in the inside Ackerman steering angle. The error between the actual and ideal inside Ackerman angle will then be computed. With multiple turning radii, the steering error for each can be determined, and the mean square error was calculated as:

$$MSE = \frac{1}{n}\sum_{i=1}^{n}\left(\theta_{i,ideal} - \theta_{i,actual}\right)^2 \tag{6.19}$$

where n is the number of tested turning radii.

This value was used to evaluate the accuracy of the steering system for the assumed dimensions. With the position analysis completed, the optimization tool in MATLAB was utilized to reduce the steering error.

The MATLAB program can be broken down into steps as follows:

Step 1: Input the wheelbase, kinematic track, and minimum turning radius

Step 2: Input the assumed dimensions for the steering system: steering arm and neutral angle

Step 3: Calculate the ideal Ackerman angle for a range of turning radii from minimum to neutral steer (infinite turning radius)

Step 4: Prescribe the outer turning angles to calculate the inner turning angles

Step 5: Calculate the mean square error for the chosen steering system parameters

Step 6: Iterate to change the steering dimension to lower the mean square error

Step 7: Stop when a criterion is met (change in MSE error between different dimensions is smaller than a set value). The optimized dimensions for the steering system have been achieved.

The full MATLAB program can be seen in Appendix C.

With the optimized dimensions selected for the track rod steering mechanism. The detail design step can be proceeded to select the components for the mechanism and determine how the system will be incorporated onto the vehicle.

Steering control system:

With the use of the track rod steering system, a steering control system must be employed as an actuator for the steering mechanism.

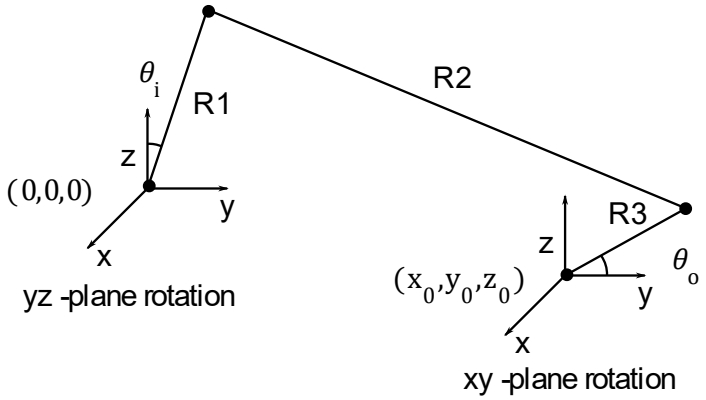

Figure 6.19: Position analysis for 3D four-bar linkage

As seen in Figure 6.19, the steering control system was modeled as a 3D four-bar linkage. Firstly, the DOF of the linkage had to be calculated. A pin restricts the 5 DOF, and a ball joint connection restricts 3 DOF. As a result, the DOF of the system can be expressed as:

$$DOF = 6(L-1) - 5J_1 - 3J_2 \tag{6.20}$$

where L is the number of links, J_1 is the number of pins, and J_2 is the number of ball joint connections.

After the required number of DOF was achieved, the input and output angle for the steering control system was analyzed. The input angle is the rotation of the lever when the user operates the steering handles. The output angle is the rotation of the steerer tube of the vehicle.

The origin is the center of rotation of the handle, and the point (x_0, y_0, z_0) is the center of rotation of the bracket connected to the steerer tube. From Figure 6.20, initial dimensions were assumed for the linkage based on the model in SolidWorks, and the input angle was prescribed for the handle. As a result, the output angle was calculated by solving the equation:

$$(x_0 - R_3 \sin\theta_o)^2 + (y_o + R_3 \cos\theta_0 - R_1 \sin\theta_i)^2 + (z_0 - R_1 \cos\theta_i)^2 - R_2^2 = 0 \tag{6.21}$$

As seen in the equation above, the only unknown is θ_0. Therefore, a function was created in MATLAB in order to solve the output angle, and the steering control system was also simulated.

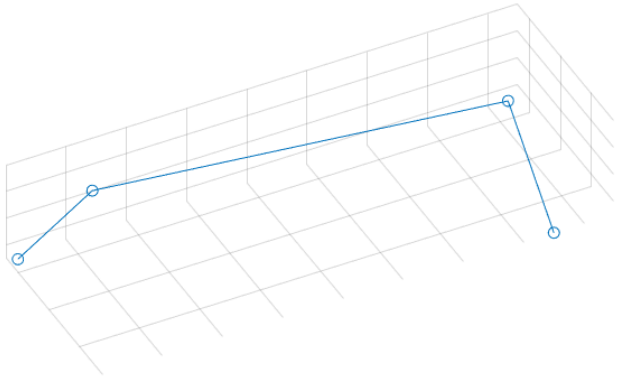

Figure 6.20: MATLAB simulation for the 3D four-bar linkage

From there, the steering sensitivity, a non-dimensional quantity, was defined as the ratio of the output angle to the input angle:

$$Sensitivity = \frac{\theta_o}{\theta_i} \tag{6.22}$$

This number represents how quickly the steer responds to the input of the user. As a result, this value is significantly user-dependent, and for an initial design, the optimal value for the sensitivity cannot be achieved. However, for further design phases, prototypes can be made, and user feedback can be utilized in order to select the best sensitivity; thus, optimizing the dimensions of the steering control system.

Detail steering design*:*

The selection of the components highly revolved around the manufacturability and the budget for the project.

The track rod mechanism is a four-bar steering linkage system. For the track rod, internal or external threaded rods can be used. Internal threaded are more resistant to bending, which creates a more robust steering system. However, they have a higher cost, and since the threads only protrude a short distance, the length of internally threaded rods from vendors are practically fixed in length. This makes internally threaded rods restrictive and difficult to achieve the optimized dimensions calculated.

On the other hand, external fully threaded rods can be cut to the correct size specified by the MATLAB program with minimal error. However, the full external threaded rods are more prone to bend; however, the forces on the steering linkage system are relatively low. As a result, the aluminum fully threaded rod was selected as the component for the track rod to also achieve low weight for the vehicle. From there, the corresponding ball-bearing rod ends were selected based on the type of thread on the rod. Figure 6.21 shows the chosen components for the track rod.

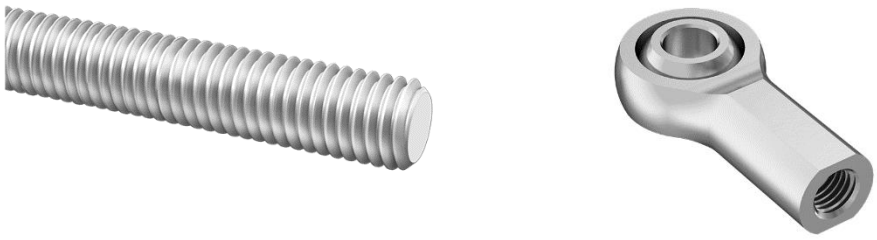

Figure 6.21: Components for the steering mechanism

The same fully external threaded rod and rod ends were also selected for the steering control linkage system for the same reason.

For the steering arms, brackets machined from sheet metal to the desired length of the steering arms can be made and welded to the steerer tube of the wheels. Since the material for the steered tube was aluminum, the bracket's material was also chosen to be aluminum for the ease of welding. The arm for the steering control can be manufactured in a similar manner. Figure 6.22 shows the steering mechanism, and Figure 6.23 the steerer tube with the welded brackets.

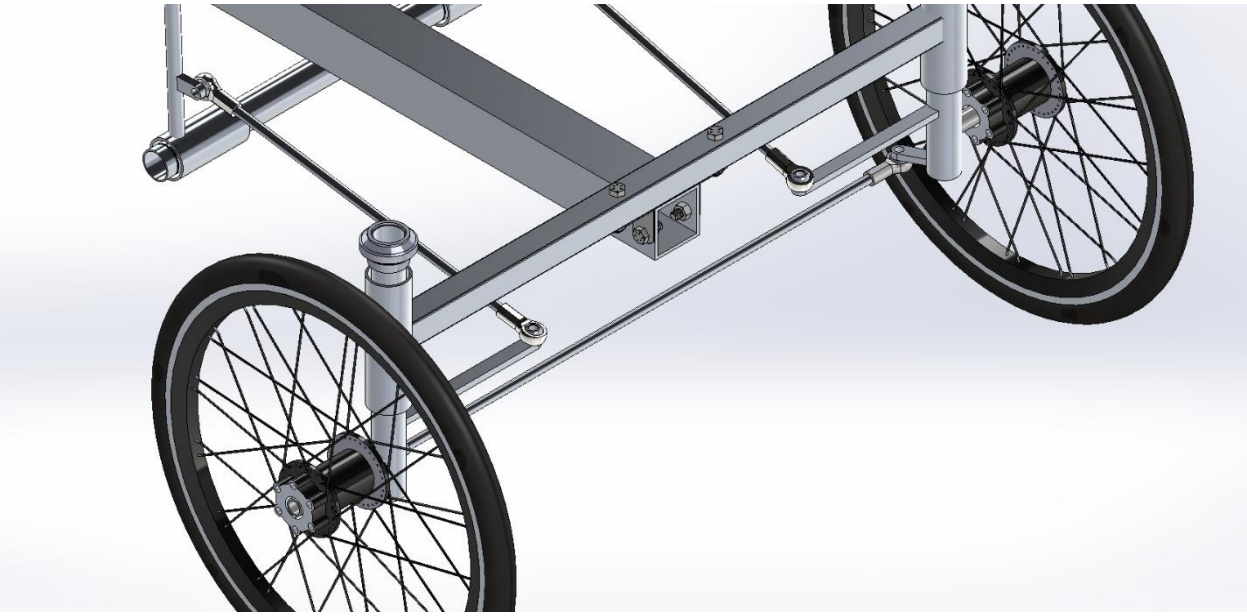

Figure 6.22: Welded brackets on the steerer tube

Figure 6.23: Brackets for the steering mechanism and the steering control

The final detail is the handle for the steering control. Figure 6.24 shows the design of the handlebar assembly.

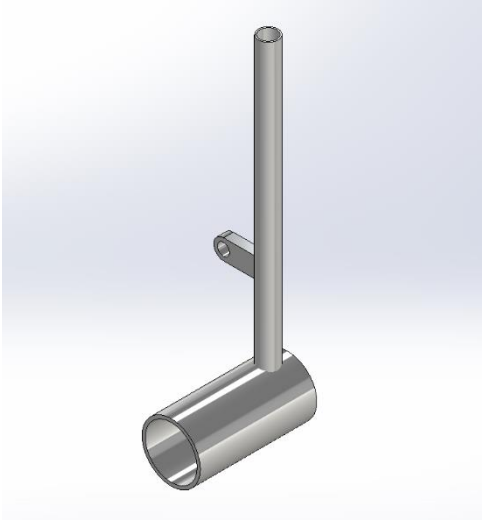

Figure 6.24: Handle to control the steering

The bracket used for the arm of the steering control system is manufactured using the same sheet metal selected for the track rod mechanism steering arm. The bracket is welded to a hollow aluminum tube to create the handle for the steering control mechanism. Bike handlebar tape can be used to wrap around the tube to protect the user from exposed metal, and it can also provide more grip for the user. The small hollow tube is welded to a lower hollow aluminum tube to be mounted onto the vehicle (Figure 6.25).

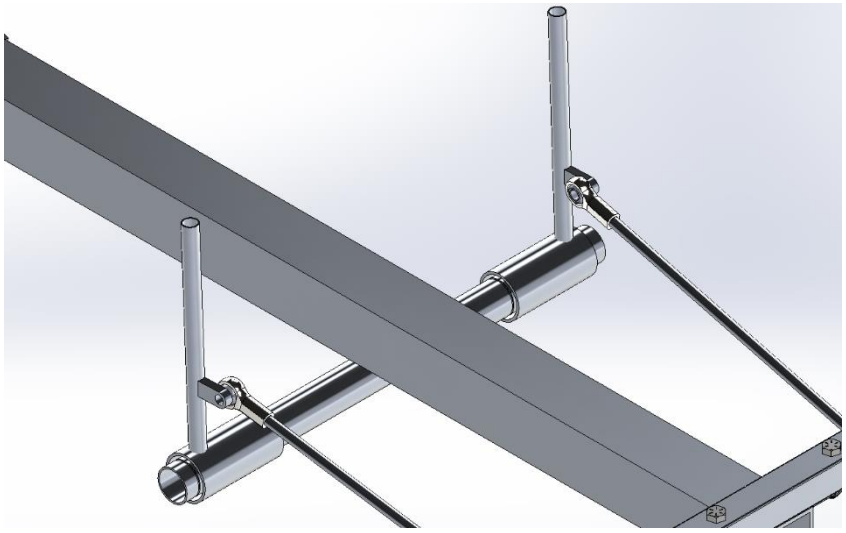

Figure 6.25: Location of the handle on the main frame

An aluminum hollow tube will be welded onto the main frame of the vehicle to provide a mounting point for the handlebar assembly. Ball bearings will be fitted inside the handlebar assembly to allow the handlebars to rotate freely around the mounting tube. Two retainer rings can be used on each side of the handlebar assembly to prevent it from moving axially along the mounting tube.

Hence, the overall steering mechanism, including the track rod steering mechanism and the steering control mechanism, is shown in Figure 6.26.

Figure 6.26: Overall steering mechanism

Drivetrain methodology:

For the drivetrain system was designed to be a simple, efficient, and effective way of propelling the vehicle. A front-wheel drive system was chosen for the vehicle to shorten the length of the chain and reduce the likeliness of jumping teeth or the need for additional chain tensions or guides. For the actual crankset and cassette, high-end gears were used for a smooth ride and easy shifting, as this vehicle could end up replacing someone's daily vehicle within a city. A crankset is the gear or stack of gears that are connected to the pedals. For the crankset, a two-gear set was utilized, with a large 50 tooth and a small 34 tooth gear. Having two gears on the crankset doubles the amount of gear ratios of the overall system. The cassette is the rear stack of gears that is connected to the hub of the wheel. These usually consist of 5 to 9 gears, and for the application, 9 gears were chosen. The gears had 11 13 15 18 21 24 30 37 46 teeth, respectively, bringing the total speeds of the bike to 18. This would allow the driver to adapt the wheel speed to perfectly fit their cadence. The shifting would be done via a wireless electronic gear selector, mounted to the steering lever. This device sends a signal to the gear changer, attached near the cassette. This would ensure that no wires or cables get in the way of the system, since it is not set up like a traditional bicycle. The drivetrain system must also have an electric assist. For the design, an electric motor was added, and it was a direct drive to the hub. This would allow the wheel to be spun by just the pedals, by the pedals and the motor, or by just the motor. The separation from the pedal driven assembly will also simplify the system for reliability and maintenance. The electric motor would be powered by stored electricity, such as a battery pack,

and activated via a throttle on the lever so that the driver always has direct control as to how much power they want from the motor.

Determining whether to put the pedals in front of or behind the front wheels was thought of carefully. Determining that the tricycle will have a better turning radius and more downwards force on the driving wheel if the pedals are the farthest out helped decide that the front wheel will be as close as possible to the rider. This provides more traction, a better turning radius, and a smaller design.

Braking methodology:

For the braking system, the vehicle was required to stop in a certain distance. There are many factors that must be taken into consideration for the braking to be done right. One parameter would be weight. The heavier the weight on the bike and person the stronger and bigger the brakes must be. Since the bike is an aluminum frame this means the overall weight would be lighter than a steel frame which would give the vehicle a better chance of braking faster. Another parameter was how fast the bike would move which means that at top speed, the stopping distance must be calculated from top speed to 0 miles per hour.

The identification of need was to pick a big enough braking system to allow the vehicle to come to a stop from 25 km/h (22.78 ft/s) in a distance of 6.0 m (19.7 ft). 2 types of braking systems were considered, a typical mechanical braking system to a hydraulic braking system.

The brake force for the vehicle was calculated using the energy theorem:

$$\frac{mv^2}{2} = F_B d \tag{6.23}$$

where m is the mass of vehicle, v is the initial velocity, and d is the required stopping distance, and F_B is the brake force.

As a result, the brake force was calculated as:

$$F_B = \frac{mv^2}{2d} \tag{6.24}$$

The brake force was calculated using:

$$F_B = \frac{\mu F_r r_{disc}}{r_{wheel}} \tag{6.25}$$

where F_r is the force at the disc brake, r_{disc} is the radius of the disc brake, and r_{wheel} is the radius of the wheel.

From there, the brake pressure was determined from:

$$P_{brake} = \frac{F_r}{A_{pad}} \tag{6.26}$$

where A_{pad} is the area of the brake pad.

The number of brakes was considered for the vehicle, which depended on both cost and safety. For the mechanical brakes considered, these were the simplest and most cost-effective systems. The mechanical brakes were going to be mounted on the front wheel and clamped down using rubbing pads into the front wheel to stop. These would be actuated with a simple lever on the steering handle. The cost is also significantly cheaper than hydraulic due to fewer components. These types of brakes are usually used on cheaper bikes as well. The stopping power of these is significantly less than hydraulic brakes as well, which would not be ideal for a vehicle of 200lbs+. Hydraulic brakes were the ideal choice to go with. These included a disc brake, disc brake hub, and single-piston caliper. Hydraulic disc brake systems are a lot more costly for the vehicles' needs, typically costing from $300 all the way up to $1000 if needed. The stopping force on these was significantly better and allowed the design to reach the goals.

7. Design Solution and Final Specifications:

Design Solution:

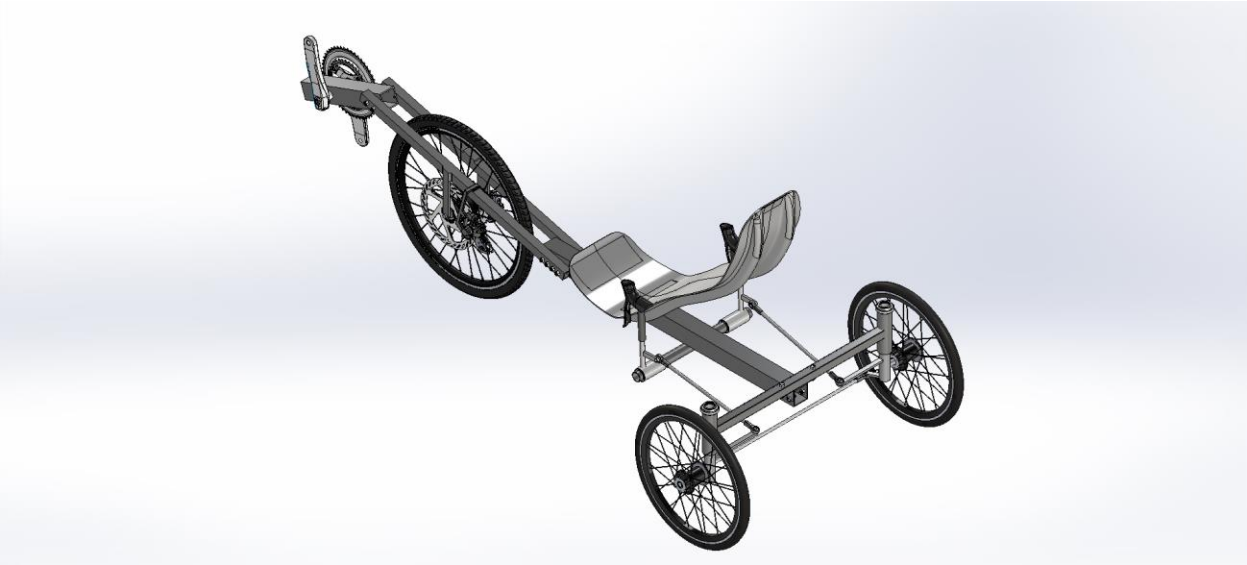

Figure 7.1: Design solution for the vehicle in SolidWorks

Table 7.1: Technical Specifications

Parameters	**Dimensions/Description**
Wheelbase	48 inches
Track	34 inches
Front wheel	22 inch/ ISO 406 mm
Rear wheels	16 inch/ ISO 305 mm
Frame Material	6061 Aluminum
Steering	Track rod mechanism
Drivetrain	18 Speed electronic shifting
Electric motor	Throttle activated direct-drive motor
Speed	20 mph top speed at 75rpm cadence
Brake	200 mm Disc Brake

The design solution is shown in Figure 7.1, and the pertinent components are shown in Table 7.1. As seen in Figure 7.1, as mentioned before, the seat of the design solution is placed close to the front in order to increase the vertical load on the front wheel. This allows for more traction on the driving wheel, which allows for better control of the vehicle.

The wheelbase and the track were designed based on similar models. However, the dimensions were iterated through testing of both the stress of the frame and the efficiency of the steering system.

The front wheel and rear wheels were selected as standardized bicycle wheels. The front wheel was selected as the ISO 406 mm, and the rear wheel was selected as the ISO 305 mm.

The frame material was selected as the 6061 Aluminum due to its lightweight and strength. The frame was designed as multiple components bolted together for ease of disassembly for transportation and shipping. Hand calculations were utilized to ensure the frame and fasteners did not yield during usage. Furthermore, FEA analysis was also conducted on the frame for the design solution for the static analysis and the low-speed collision analysis. The low-speed collision was conducted based on CFR Part 16, 1512.14. The factor of safety for both cases was greater than 1; therefore, the solution meets the requirements for the frame.

The track rod steering system was chosen for the steering mechanism since it requires fewer parts while still being effective. The parts for the steering mechanism are standardized (threaded rods and ball joint rod ends). Therefore, these components can be sourced directly from vendors, and no customized design is required. Hence, the design solution utilized the track rod steering system to minimize the cost of manufacturing and assembly.

The dimensions for the steering system were optimized through MATLAB (Appendix C). Additionally, the steering control system was also modeled using MATLAB, and the dimensions can further be iterated through user feedback to optimize the steering sensitivity.

For the drivetrain, a 156mm two gear crankset and a nine-gear cassette were chosen. The same size and teeth were used, as specified in the methodology, as this is standardized in the bike industry and makes it easy to receive through suppliers. For the electric motor, a small 350-watt

scooter motor was selected in order to keep the vehicle in the class 2 of electric bicycles. an onboard lithium-ion battery pack was chosen for the motor.

The braking system consisted of a single 200mm disc. This was used with a single-piston caliper. Hydraulically powered brakes were chosen for this setup and allowed the vehicle to get great theoretical results. The piston caliper would have an integrated hydraulic fluid reservoir to help alleviate complications with mounting and external fluid tanks taking up space.

Prototype:

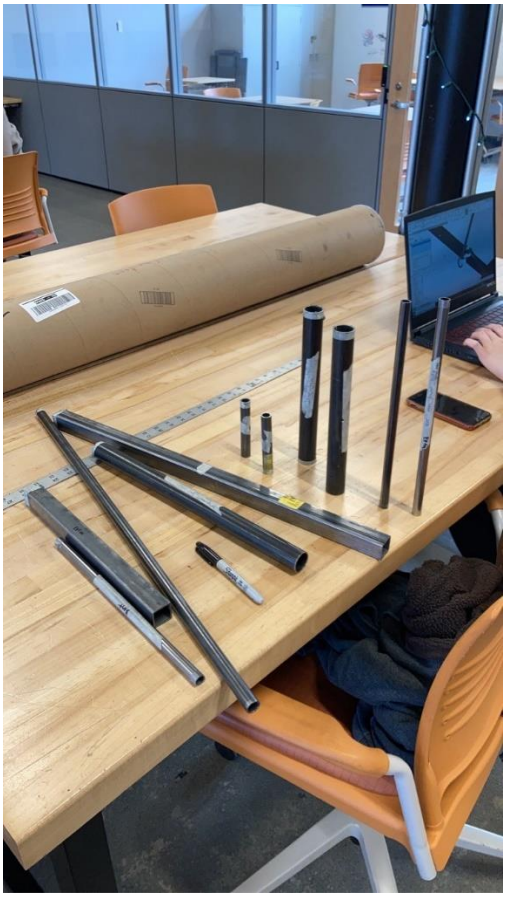

Figure 7.2: Metal stock cut to specifications

Figure 7.3: All pieces welded together into sub-assemblies

Figure 7.4: Headset bearings pressed into headsets

Figure 7.5: Threaded rods cut to length and prototype fully assembled and bolted together

Figure 7.6: Final result of prototype, cardboard wheels laser cut for demonstration and steering stops added to prevent linkage from going in reverse.

8. Results:

Frame stress analysis:

The factor of safety for the stress of the bolts and bending of frame were calculated for the static analysis using the equations in the design methodology section, and Table 8.1 shows the summary of the factor of safety.

Table 8.1: Factor of safety for components on the frame

Factor of safety of the front bolts	5.99
Factor of safety of the frame bearing stress	12.86
Factor of safety for the bending of the front bars	3.01
Factor of safety for the rear bolt in tension (proof strength)	1.33

Sample calculations are shown in Appendix D, and MATLAB code in Appendix C. As seen in Table 8.1. The factor of safety for the bending of the frame and the shearing of the bolts are all greater than 1. As a result, the static analysis showed that the frame will not yield during usage, and the fasteners will also function correctly.

The factor of safety of the frame bearing stress was high than the others since the bearing force is distributed across the thickness of the main frame and the front bars of the vehicle. Therefore, the bearing stress resulted in a low value.

FEA Modeling:

In addition, to hand calculations for the stress analysis, FEA modeling was also utilized in order to validate the static stress analysis, and it was also utilized for the low-speed impact simulation.

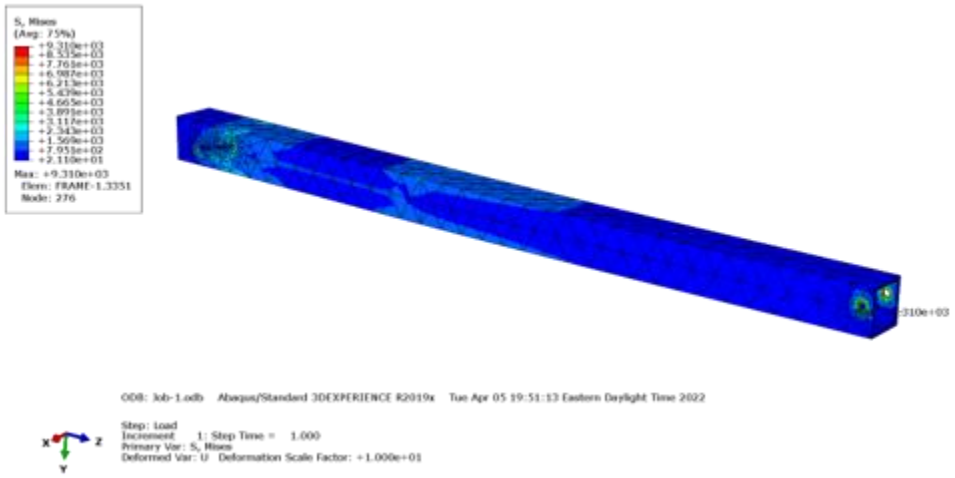

Figure 8.1: Static analysis for the main frame

Figure 8.1 shows the stress distribution for the static analysis of the main frame. As seen in the figure, the majority of the stress occurs at the location of the support, where the bolts are inserted. However, the maximum stress for the main frame only reached 9.31 ksi, which is well

below the yield strength of aluminum 40 ksi. As a result, the main frame will not yield during usage.

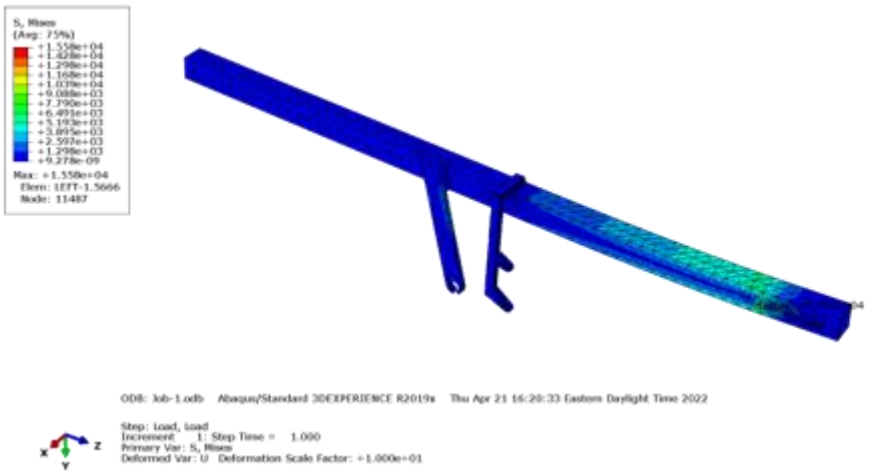

Figure 8.2: Static analysis for the front left bar

Figure 8.2 shows the FEA modeling of the front left bar of the frame. Similarly, the front right bar also had the stress concentrated at the supports. For the maximum stress was determined to be 15.6 ksi, which results in a factor of safety of 2.56. Therefore, the front left frame was designed correctly to withstand the forces.

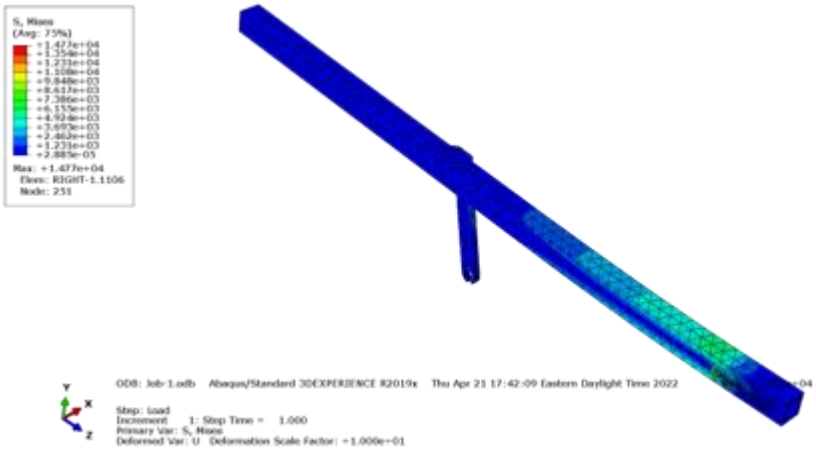

Figure 8.3: Static analysis for the front right bar

Figure 8.3 shows the FEA modeling of the front right bar of the frame. The maximum stress for the component resulted in 14.3 ksi, which is equivalent to a factor of safety of 2.80. As a result, the front right bar will not yield when being used.

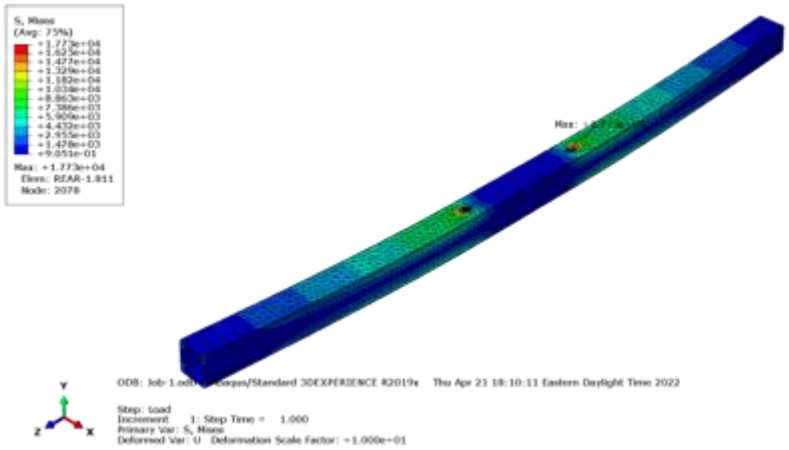

Figure 8.4: Static analysis for the rear frame

Figure 8.4 shows the FEA modeling of the rear frame of the vehicle. The maximum stress of the rear frame from the simulation in Abaqus was 17.7 ksi. Therefore, the factor of safety for the rear frame was 2.26. Thus, the rear frame was also designed to sufficiently support the vehicle.

In addition, to modeling the static analysis, the low-speed collision was also analyzed using Abaqus through the CPSC standard for bicycle frame testing. A horizontal load of 200 lb was applied for the components, and the stress distribution was evaluated.

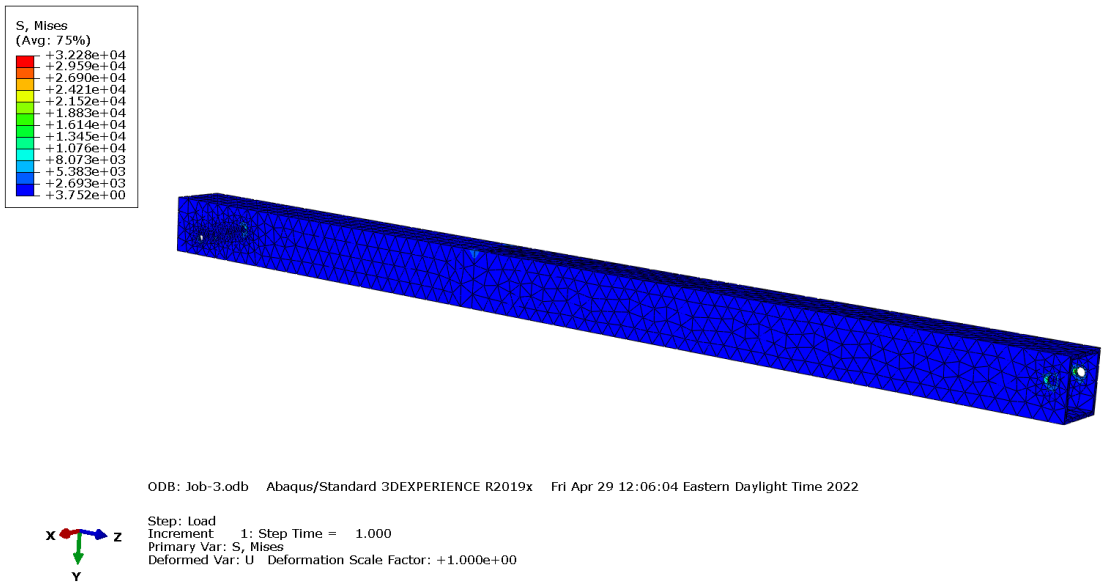

Figure 8.5: Low-speed collision analysis for the main frame

Figure 8.5 shows the stress distribution of the frame. The maximum stress for the main frame reached 32.2 ksi for the low-speed collision simulation. This value was substantially higher than the maximum stress obtained from the static analysis (9.31 ksi). However, the stress was still lower than the yield strength of 6061 Aluminum, which showed a safety factor of 1.24. As a result, even in a low-speed collision, the main frame will not yield.

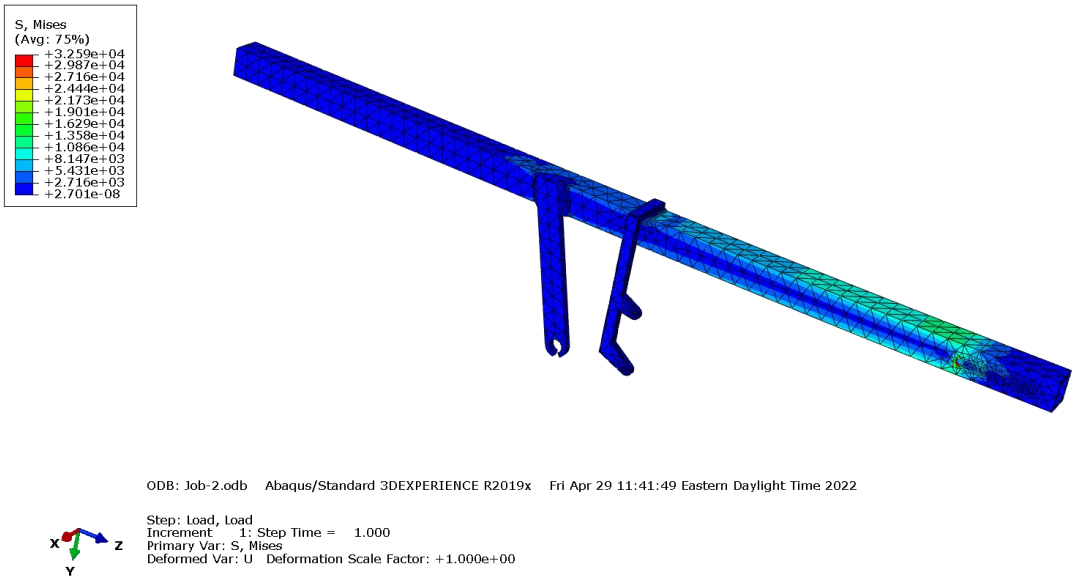

Figure 8.6: Low-speed collision analysis for the front left bar

Figure 8.6 shows the front left bar for low-speed collision analysis using FEA. As seen in the figure, the maximum stress was increased significantly and resulted in 32.6 ksi. The factor of safety was calculated as 1.23, and this showed that the bar would not deform plastically during a low-speed collision.

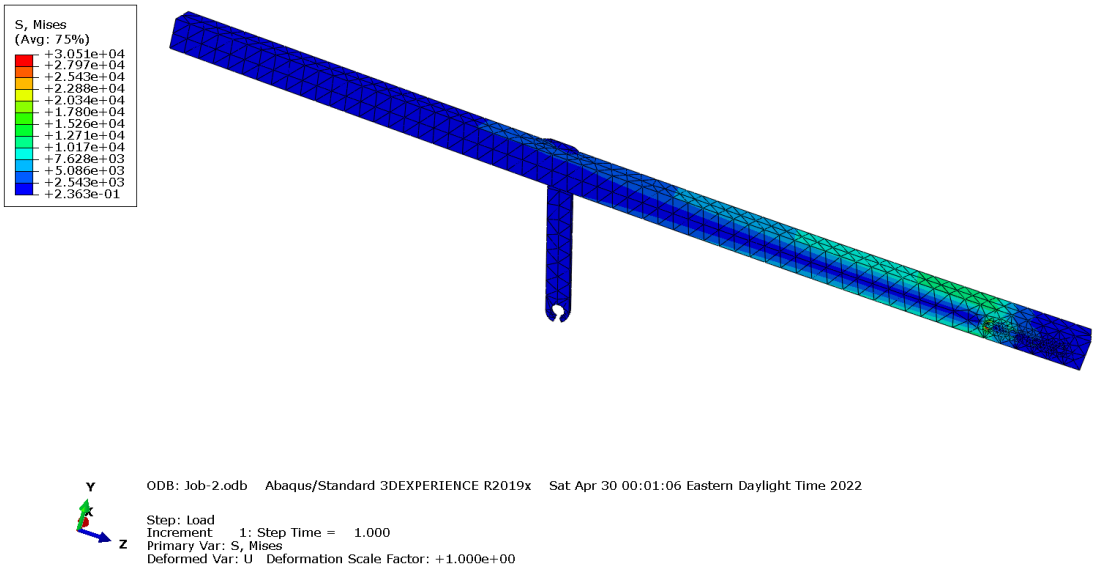

Figure 8.7: Low-speed collision analysis for the front right bar

Figure 8.7 shows the right bar for low-speed collision analysis using FEA. The maximum stress for the right bar was determined as 30.5 ksi, which is equivalent to a factor of safety of 1.31. Hence, the front right bar was designed correctly to withstand a low-speed collision.

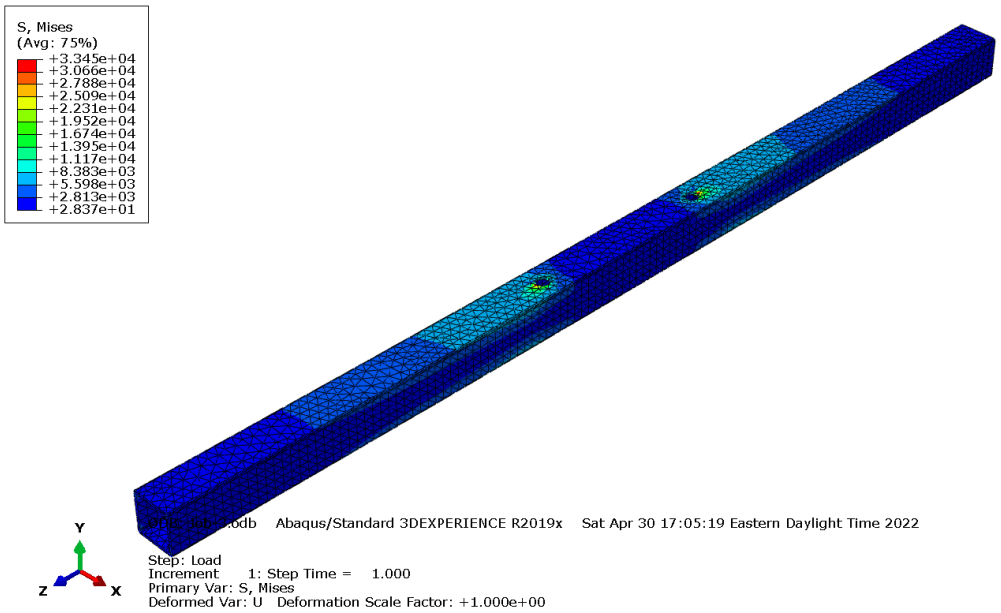

Figure 8.8: Low-speed collision analysis for the rear frame

Finally, Figure 8.8 shows the low-collision analysis for the rear of the vehicle. The maximum stress, 33.5 ksi, for the rear frame was located at the supports. The factor of safety was calculated as 1.20. Thus, the rear frame will not yield during a low-speed collision.

Steering system:

For the steering system with the wheelbase and the kinematic track designed, the steering arm and the track rod length were readily determined. These parameters were chosen to minimize the mean square error of the steering angle using MATLAB.

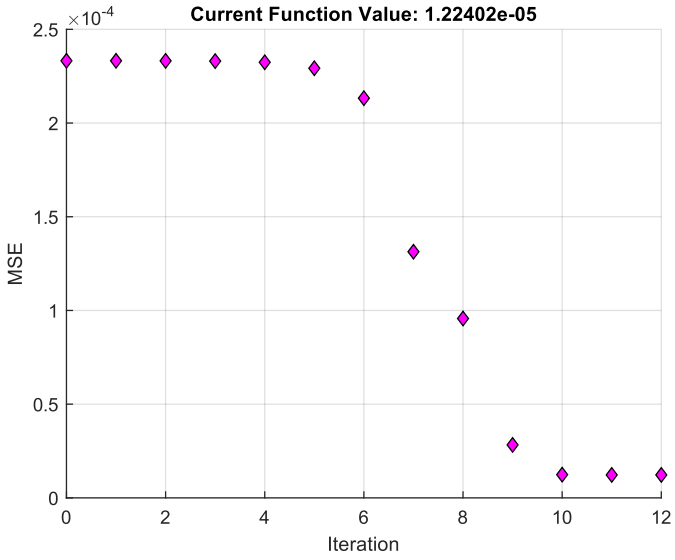

Figure 8.9: Optimization function to minimize the steering angle

Figure 8.9 shows the iterations of the optimization function utilized in MATLAB. The function required 12 iterations to converge, and the final mean square error was reduced to only $1.22 \times 10^{-5}\ deg$.

The four-bar linkage was also simulated in MATLAB to visualize how the motion of the steering system would appear to be.

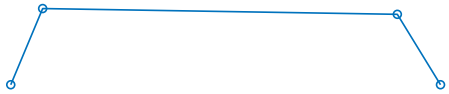

Figure 8.10: Simulation for the track rod steering system in MATLAB

The optimized dimension for the track rod steering system is shown in Table 8.2.

Table 8.2: Optimized dimensions for the track rod steering system

Component	Length
Track Rod	31.8 inch
Steering Arm	2 inches

Since the MSE error of the steering angle is small, the vehicle certain can turn within a radius of 26.2 ft, which satisfies the design requirement in Table 1.

Steering control:

The steering control system was also modeled using MATLAB in order to visualize the motion of the 3D linkage.

The dimensions for the 3D linkage steering control system are shown in Table 8.3.

Table 8.3: Dimensions for steering control

Component	Length
Lever	3 inches
Steering Link	14.4 inch
Steerer Tube Bracket	6.5 inch

The system resulted in a steering sensitivity of 0.42, which is the ratio of the rotation of the steerer with respect to the input rotation from the handlebar lever. This value is difficult to

optimize using only simulation since it is highly dependent on user experience. As a result, the value was only chosen as a starting point for the prototype. However, in the future, when testing is conducted with the feedback of users, this value can be determined more concretely, and the dimensions for the steering control system can be iterated from there.

Drivetrain analysis:

For the drivetrain analysis, a simple MATLAB code was written to calculate the gear ratios of the system and the approximate wheel speed of the vehicle at a 75-rpm cadence, or pedal speed. The 75-rpm cadence was chosen because it is at the high end of an amateur's pedal speed and the low end of a professional's speed. The calculated ratios and wheel speeds are shown in the table below. This satisfies the electric bicycle class 2 specifications and maximum speed.

Table 8.4: Drivetrain system and speed

Gear ratios									
Teeth	11	13	15	18	21	24	30	37	46
34	0.324	0.382	0.441	0.529	0.618	0.706	0.882	1.088	1.353
50	0.220	0.260	0.300	0.360	0.420	0.480	0.600	0.740	0.920
Wheel Speed (mph)									
Teeth	11	13	15	18	21	24	30	37	46
34	13.79	11.67	10.11	8.429	7.225	6.322	5.057	4.101	3.298
50	20.28	17.16	14.87	12.396	10.625	9.297	7.437	6.030	4.851

Brake Analysis:

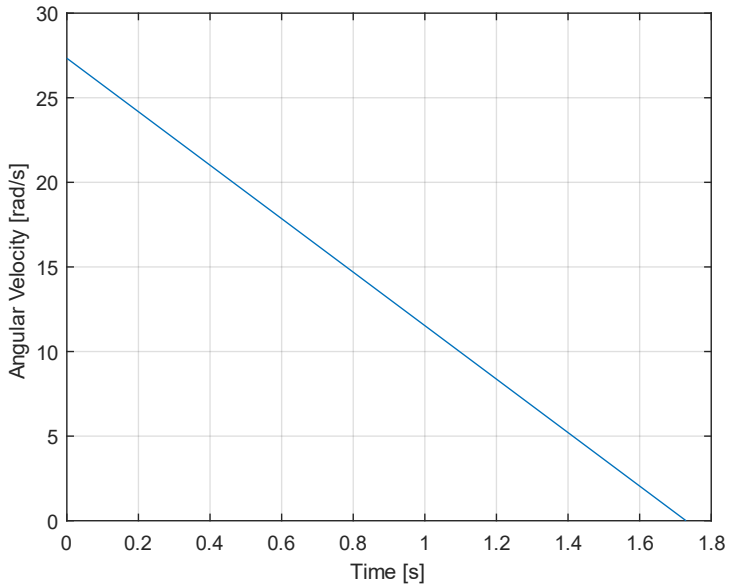

Figure 8.11: Wheel stop time

Table 8.5: Brake pressure vs recommended brake pressure

Required brake pressure (psi)	**Recommend brake pressure (psi)** [8]
1020.4	1000 - 1200

Table 8.5 shows the required brake pressure to stop the vehicle and the recommended brake pressure. 200 mm brakes were chosen for the vehicle. Applied to this disc was a single-piston caliper. The brake force needed was attained. The MATLAB simulations showed the required brake pressure needed to stop the vehicle was 1020.4 psi which was well in the range of the 1000-1200 psi needed.

Drag analysis:

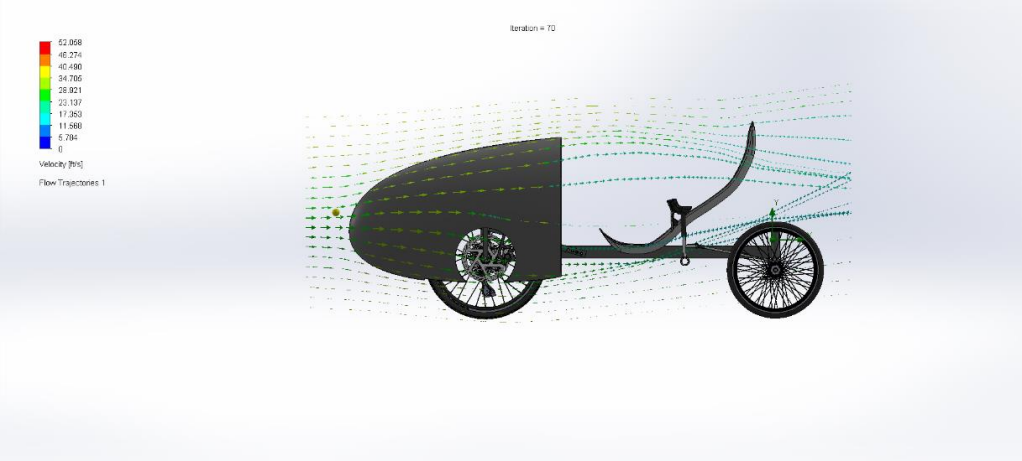

Figure 8.12: Flow through the vehicle with front fairing

A drag analysis was conducted for a front fairing. Since the drag for a user with was difficult to model using a CFD software due to the complexity of modeling a human, the drag coefficient for the simulation of the front fairing will be compared to a drag coefficient of a bicycle with a user. [2].

The comparison is shown in Table 8.6.

Table 8.6: Drag coefficient of bicycle vs the designed vehicle with front fairing

	Standard Bicycle	**Vehicle with front fairing**
Drag Coefficient	0.88	0.25

As seen in Table 8.6, the drag for the vehicle with front fairing drastically reduced the drag coefficient compared to a normal bicycle with a human. However, this comparison was only an approximation since the drag coefficient for the vehicle itself with a human was not determined. As a result, the fairing was not chosen for the final design. However, the results of the comparison show promising drag reduction if front fairing was employed. In the future, when an accurate model for the user can be implemented into the vehicle, the drag coefficient can be studied further, and the decision of whether a front fairing would improve the aerodynamic quality of the vehicle can be readily made.

9. Risk Assessment:

The risk severity matrix seen below in Table 9.1 and Table 9.2 outline the risks that the team predicted could happen. The two greatest risks to the project were falling behind on schedule and the team's construction ability. The reason that not staying on schedule was so crucial is that this project was over one semester which is short and with only 4 team members there is a lot of work to do in a little time. Staying focused and sticking to the plan was required to achieve desired results. The construction ability was the next biggest risk, the team was unsure if access to a welder was available, so the frame was designed with bolts. The ability to put together the

prototype was highly dependent on timing and required experimenting and testing. Having a team member who does not produce was another risk. With only four members on the team to build this vehicle the necessity to have everyone highly involved is very high. The team mitigated this risk by being inclusive and letting people choose what parts of the project that most interested them. With the fast paced one semester project the team had to be focused and willing to put in the work.

The design of the tricycle is likely to work but there would be some safety risks with the current design as it is now. With not enough time to design a rollbar or a harness, there are potential hazards for rolling over or slipping out of the seat on a tight turn. There is also the risk of sliding into the wheel or touching the wheel with the legs while the users are pedaling. These potential points of failure in the category of safety would be addressed if the project were to be worked on more. The low risk of the battery malfunctioning and getting too hot is also a possibility, this could be avoided by extra research and protecting the battery with a cover. For the design, the risks were low and the team was able to produce an accurate CAD model and a prototype of the steering system and frame.

Table 9.1: Risk Assessment Matrix

Risk Severity Matrix			
	ACCEPTABLE	TOLERABLE	GENERALLY UNACCEPTABLE
NOT LIKELY		4	
POSSIBLE	2	6 & 7	5
PROBABLE	1	3	

Table 9.2: Risk Mitigation Plan

#	**Risk Identification**	**Mitigation Plan**
1	Lack of time to build prototype	Create a full CAD model
2	Insufficient funds to build	Build appropriate prototype
3	Having to redesign the prototype	Consult with professor before moving onto construction
4	Falling behind schedule	Follow the action plans and keep team members accountable
5	Construction ability	Bolted frame instead of welded frame
6	Team member unable to produce	Support them and give them a task that is suited towards their strong abilities
7	Material lead time	Purchase material on time and early if necessary

10. Detailed Cost Analysis:

The complexity of the project and a smaller budget prevented the team to build a full prototype. However, a bill of materials was created for a fully built tricycle. The bill of materials in table 13. has a detailed account of everything that would've been purchased to build the Turbo Trike. Most of the components can be found at local stores and online at various websites. The large cost of the project is since the Turbo Trike is a high-end bike meant for racing or consistent daily driving. With its strong structure and high-quality drivetrain system, the tricycle is meant for a serious rider.

Table 10.1: Cost Analysis

Part	QTY	Unit of measurment	Part Number	Price per	Price Total
High-Strength Grade 8 Steel Hex Head Screw	6	each	91268A512	$ 2.88	17.28
High-Strength Steel Nylon-Insert Locknut	1	bag of 25	90630A110	$ 4.49	4.49
High-Strength Grade 8 Steel Hex Head Screws	1	bag of 10	91268A505	$ 8.61	8.61
Multipurpose 6061 Aluminum Rectangular Tube, 1/8" Wall Thi	1	3 feet	6546K23	$ 61.14	61.14
Multipurpose 6061 Aluminum Rectangular Tube, 1/8" Wall Thi	1	12 inches	6546K23	$ 29.00	29.00
Multipurpose 6061 Aluminum Rectangular Tube 1/8" wall thickness 1" high x 1" wide (60 inches)	1	60 inches	6546K21	$ 54.16	54.16
Spoked Hollow-Tread Flat-Free Wheels	2		2893T71	$ 64.75	129.50
Spoked Hollow-Tread Flat-Free Wheels	1		22585T48	$ 71.40	71.40
Trike seat	1		http://www.thorseat.eu/e	$ 250.00	250.00
High-Strength 6013 Aluminum Sheet 1/2" thick (for bracktes)	1	8"x8"	9050K15	$ 57.49	57.49
General Purpose Aluminum Tubing (2ft) 1-1/2" OD, .083" wall thickness	2	2 ft	9390N35	$ 20.18	40.36
General Purpose Aluminum Tubing 1-1/8" OD, .058 wall thickness	1	6 ft	9390N21	$ 54.25	54.25
General Purpose Aluminum Tubing 5/16"-18 thread size, 4 feet long	1	4 ft	94435A519	$ 9.75	9.75
FSA TH-855 Headset	2	each	https://www.amazon.com	$ 18.98	37.96
Lubrication-Free Ball Joint Rod End	6	each	2458K33	$ 6.73	40.38
SHIMANO ULTEGRA HOLLOWTECH II Crankset 2x12-speed	1		https://bike.shimano.com/	$ 290.00	290.00
SHIMANO ULTEGRA 12-speed HYPERGLIDE+ Road Cassette Sprocket	1		https://bike.shimano.com/	$ 111.99	111.99
Shimano XT/Ultegra 12-Speed Chain Silver, 126 Links	1		https://www.amazon.com	$ 69.99	69.99
SHIMANO DEORE XT CENTER LOCK Disc Brake Rotor 203/180/160/140 mm SM-RT81	1		https://bike.shimano.com/	$ 44.95	44.95
SHIMANO ULTEGRA Hydraulic Disc Brake Caliper BR-R8170	1		https://bike.shimano.com/	$ 82.99	82.99
SHIMANO ULTEGRA Di2 Rear derailleur SHIMANO SHADOW RD 2x12-speed RD-R8150	1		https://bike.shimano.com/	$ 286.99	286.99
SHIMANO ULTEGRA Di2 Rim Brake DUAL CONTROL LEVER 2x12-speed (ST-R8150-L)	1		https://bike.shimano.com/	$ 213.99	213.99
SHIMANO ULTEGRA Di2 Rim Brake DUAL CONTROL LEVER 2x12-speed (ST-R8150-R)	1		https://bike.shimano.com/	$ 213.99	213.99
SHIMANO ULTEGRA Di2 Front Derailleur 2x12-speed (FD-R8150)	1		https://bike.shimano.com/	$ 259.99	259.99
SHIMANO ULTEGRA Threaded Bottom Bracket 68/70 mm shell width SM-BBR60	1		https://bike.shimano.com/	$ 31.99	31.99
36 Volt 350 Watt MY1016 Electric Motor with 11 Tooth #25 Chain Sprocket & Bracket for Scooters	1		https://www.monsterscoo	$ 53.99	53.99
US Warehouse) 72v/60v/48v/52v/36v/24v Ebike Battery for 250w -3000w Motor, 15Ah/20Ah/25Ah	1		https://www.amazon.com	$ 341.00	341.00
engineering cost	1			$ 960.00	960.00
				Total cost	3,827.63

This is the first year a team has worked on this project at UMass Lowell so there was no background to go off. From scratch, the bike costs a lot more than it would if it was produced in a facility. The estimated project hours for the design, fabrication, testing, and documentation of the Turbo Trike are seen below.

8 hours per week * 4 students * 12 weeks = 384 hours
384 hours * 25 $/hour = $9600

Assuming ten models of the Turbo Trike were built, the added engineering cost to the trike would be $960. With this added cost the Turbo Trike still is very competitive in its market for

the features it has. The gearing and shifting components a bike have can vary the cost of a bike by a large margin. For the Turbo Trike, the top-of-the-line Shimano Ultegra group set with electronic shifting was selected. This high-end group set gives the rider a smooth transition when shifting gears and it has plenty of gears for going uphill or downhill to make the rider's experience more enjoyable. As seen below in Table 10.2 there is a comparison between the cost of the Turbo Trike and other models that are on the market.

Table 10.2: Vehicle comparison

Model	Cost	FWD or RWD	Electric motor	Battery size	Gearing (high quality, medium quality, low quality, single speed)
Turbo Trike	$ 3,827.63	FWD	Yes	350 Wh	high quality
Ice VTX	$ 7,150.00	RWD	No	0	high quality
Mobo triton pro	$ 419.99	FWD	No	0	single speed
Outrider Transition	$ 5,850.00	RWD	Yes	1144 Wh	medium quality
Catrike 5.5.9 eCat	$ 5,950.00	RWD	Yes	400 Wh	low quality

The Turbo Trike is more than $1000 less than the model that is most like it. There is only one model that is cheaper than the Turbo Trike and that is the Mobo Triton Pro tricycle. The Mobo Pro tricycle only has one gear so the user cannot shift and has a slow top speed. The frame is well built but they achieved the low cost by not making it a practical bike to commute or race. When comparing the Turbo Trike to the other models on the market, it has a smaller battery than the other brands which could account for some of the reasons it is cheaper. Overall, it is similar and still has a lower price point with a very high-quality gearing setup. In Figure 10.1 below, the difference of price the trikes in the market today are shown.

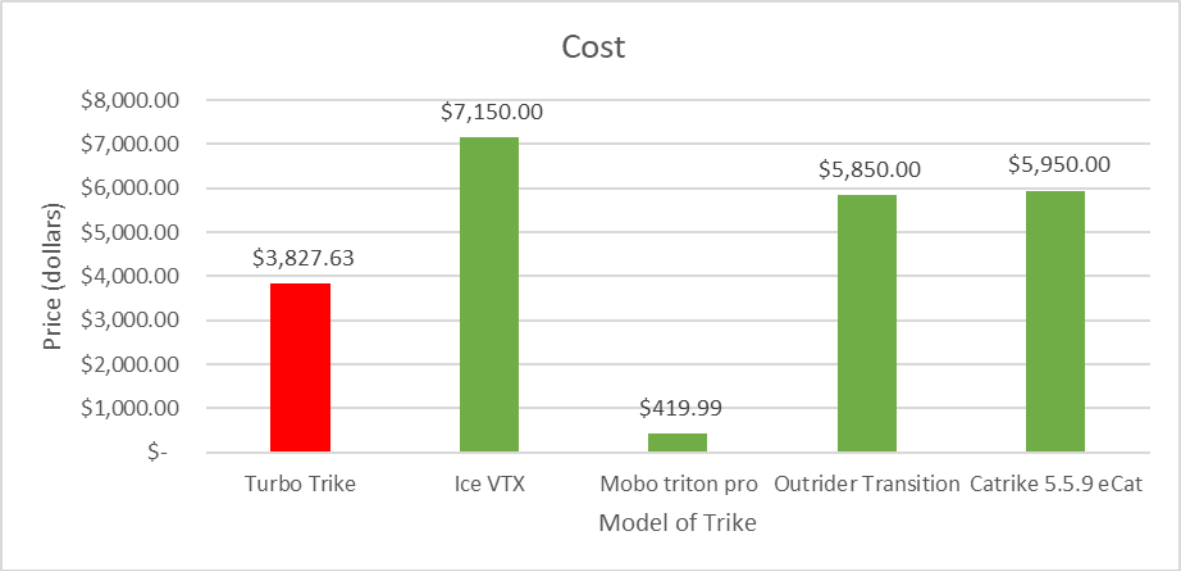

Figure 10.1: Cost comparison between models

The Turbo Trike at a lower price level and high-performance level would be ideal for the tricycle racing enthusiast or even someone looking to commute to work on a recumbent bike. By saving gas by driving a combustion vehicle the Turbo Trike remains a practical option for people of all ages and sizes to be able to save some money and still get where they need to go. The cost analysis would change with further iterations of the trike but one of the goals is to help keep the Turbo trike accessible to everyone. To make the Turbo Trike more accessible it is easy to offer

different gearing packages on the vehicle so a beginner can get a cheap beginner drivetrain and a racer can get a racing drivetrain. This will allow the user to select what is best for them and save them money.

11. Broader Impacts:

The design solution of the Turbo Trike has made an impact in many ways. In a global way, the design brings together manufacturers from all over the globe to get the best parts that will work and be reliable. Sourcing the parts from the best manufacturers allows for a global impact of putting money into the economy of other countries. If the Turbo Trike were to upscale manufacturing, it could be used in every country in the world. The versatile trike would be great for poor countries where they cannot afford a car and still need to commute a long distance. The easy rechargeable battery allows the trike to be a daily commuter trike that can reach high speeds and reach the destination in a timely manner. With the option to select different drivetrains, the Turbo Trike is suitable for dirt roads, paved roads, bumpy terrain, and much more. The different drivetrain selections can make the vehicle more appealing to those in poor countries that need a cheaper option.

From an economic standpoint, the Turbo Trike can make a big difference. A lot of consumers globally now want electric cars, but the high cost of a brand-new vehicle is keeping consumers from switching to renewable energy. With the battery and motor in the Turbo Trike the ability to start out in the renewable energy space is available to everyone. This will save the average consumer money on gas and maintenance that a combustion vehicle requires. With the ability to mount many attachments to the frame of the vehicle, the Turbo Trike is versatile, and money can be saved with lower cost components. This also will put money onto the local economy and have more people going into bike shops to purchase a trike. The economic impact of the Turbo Trike can be large and important.

In environmental and social contexts, the Turbo Trike will make a difference. By having renewable energy that is clean the Turbo Trike will reduce the amount of gas that is being used which will reduce the carbon footprint on the planet. Most parts of the vehicle can be recycled and reused in some way since aluminum is such a versatile metal. The battery is the one thing that creates toxic waste once it becomes unusable but recently there have been more and more companies taking old batteries and making them new again. The environmental impact the vehicle has is a beneficial impact and appeals to consumers of this day and age. Socially the Turbo Trike will turn a lot of heads and get people into the exercise commuting space. Recumbent bikes are not prevalent nowadays since they are not easily accessible. With the easily accessible, versatile Turbo Trike many new customers are going to get into the space of riding a recumbent trike to work. Once people realize that their workmates are getting to work faster by not sitting in traffic and getting in shape everyone will want a Turbo Trike. The possibilities are endless for lives this vehicle can change and it can impact the world.

12. Summary and Conclusions:

In conclusion, a human powered vehicle with electric assist was designed based on the ASME competition requirements. Multiple factors were considered, including global, economic, environmental, and social context, to design the delta tricycle that is fast, reliable, safe, and user-friendly, and the vehicle satisfied the required specifications. The design was focused on the frame, steering, drivetrain, and brakes for the vehicle, and engineering analyses were conducted using MATLAB and FEA simulations. A partial prototype was built successfully; however, more funding was needed to manufacture the whole model. Additionally, an analysis was conducted to assess the risk associated with the project, and the estimated cost of the vehicle was also compared to similar products on the market.

13. Recommendations for Further Study:

Although the goals were met for the vehicle, it was not fully built. There are a lot of improvements that could be made if the team was to design this project further. A recommendation for further study would be to focus more on the ability of steering. Another aspect that can be improved upon is the shock absorbing ability of the wheels and frame. With the stiff seat and no suspension, the rider would have a bumpy ride so incorporating that into the project would be recommended.

Additionally, a roll bar system can be employed for the safety of the rider. Details on testing can be found within the AMSE rule for human powered vehicle. Furthermore, more detailed drag analysis can be conducted with a human model for the vehicle. From there, the drag for the vehicle with and without a fairing can be compared to decide whether the fairing is appropriate. The steering system can also be optimized further by gaining feedback from users to iterate on the steering sensitivity. To achieve better steering quality, a six-bar linkage could also be tested for the steering control system if more funding is provided.

14. Bibliography

[1] C. Mark Archibald, *Design of Human-Powered Vehicles-ASME*, 1st ed,2016

[2] A. Gerhart, J. Hochstein, P. Gerhart, *Munson, Young and Okiishi's Fundamentals of Fluid Mechanics*, 8th ed, 2015

[3] *E-HPVC: Human powered vehicle challenge Fests*. [Online]. Available: https://efests.asme.org/competitions/human-powered-vehicle-challenge-(hpvc). [Accessed: 27-Apr-2022].

[4] *Prior art, Jetrike.Com - Prior Art*. [Online]. Available: https://www.jetrike.com/prior-art.html. [Accessed: 27-Apr-2022].

[5] "This a description of how to build a rear wheel steering front wheel drive trike.," *How to build a Rear Wheel Steering Front Wheel Drive Trike.* [Online]. Available: http://www.ihpva.org/projects/tstrike/rws.htm. [Accessed: 27-Apr-2022].

[6] B. Chu, *Giant CT 102 to front wheel drive delta trike conversion*, *Proporzione Divina*, 17-Apr-2011. [Online]. Available: https://proporzionedivina.wordpress.com/2011/03/18/giant-ct-102-to-front-wheel-drive-delta-trike-conversion/. [Accessed: 27-Apr-2022].

[7] *Shimano Dura Ace Di2 9200 groupset.* https://grabcad.com/library/shimano-dura-ace-di2-9200-groupset-1

[8] *How Much Pressure Does A Hydraulic Bike Brake Exert.* https://bikehike.org/how-much-pressure-does-a-hydraulic-bike-brake-exert/

[9] R. Budynas, K. Nisbett, *Shigley's Mechanical Engineering Design*, 10th ed, 2014

[10] R. Norton, *Design of Machinery*, 6th ed, 2020

[11] *Trix*. https://www.hasebikesusa.com/trix-kids-recumbent-trike.html

[12] *Mobo Triton Pro*. https://www.mobocruiser.com/MoboTritonPro-p/tri-501.htm

[13] *KETTWIESEL ALLROUND.* https://www.hasebikesusa.com/kettwiesel-modular.html

[14] *Trigo*. https://www.hasebikesusa.com/trigo.html

[15] *KETTWIESEL EVO STEPS*. https://www.hasebikesusa.com/kettwiesel-evolution-evo-steps-recumbent-trike.html

Appendix A – Complete Drawings

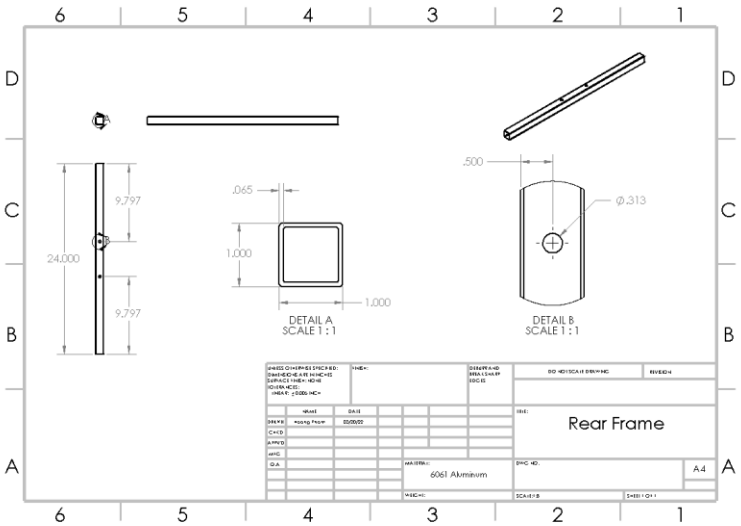

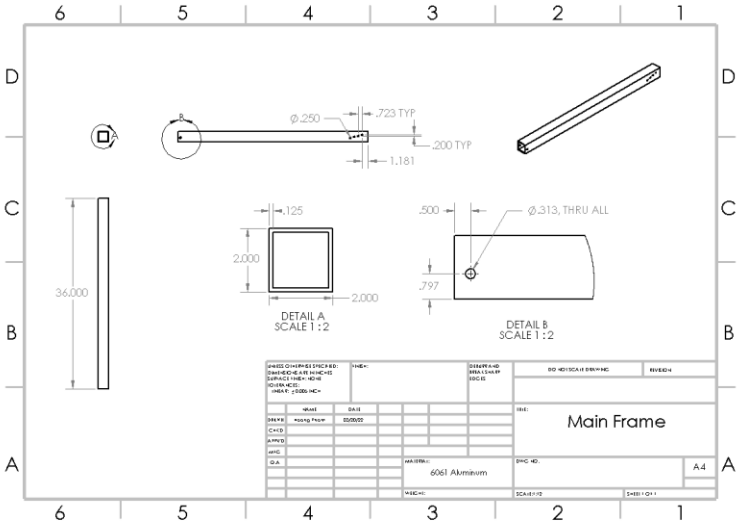

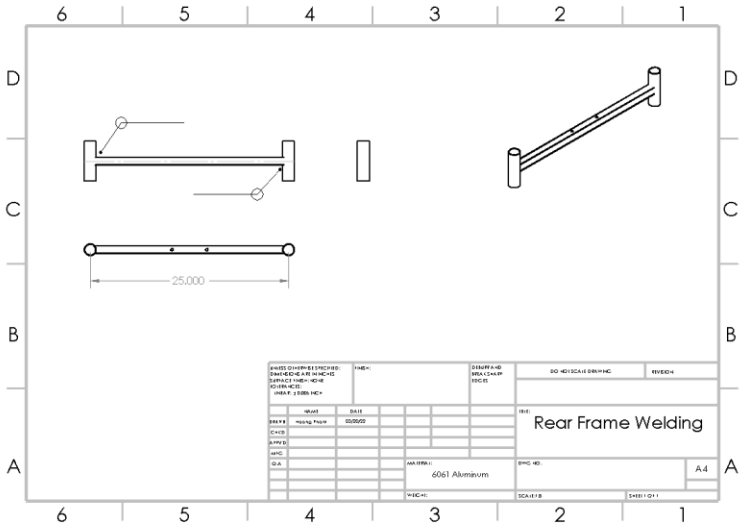
25.000
Rear Frame Welding
6061 Aluminum
A4

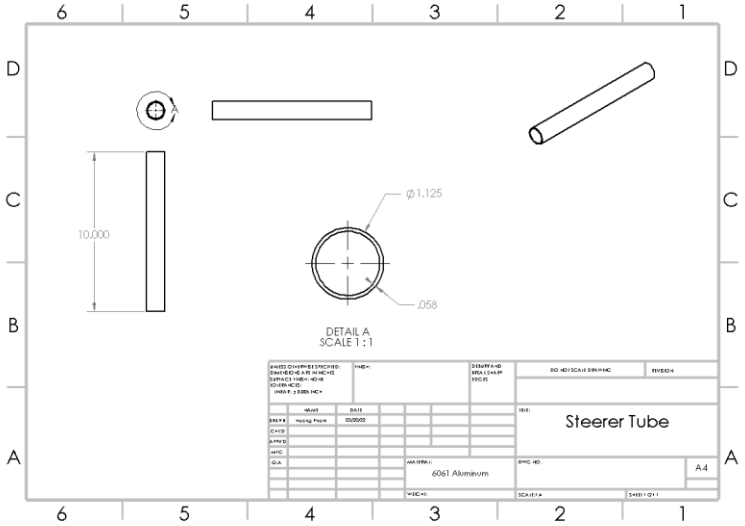
10.000
ϕ1.125
.058
DETAIL A
SCALE 1 : 1
Steerer Tube
6061 Aluminum
A4

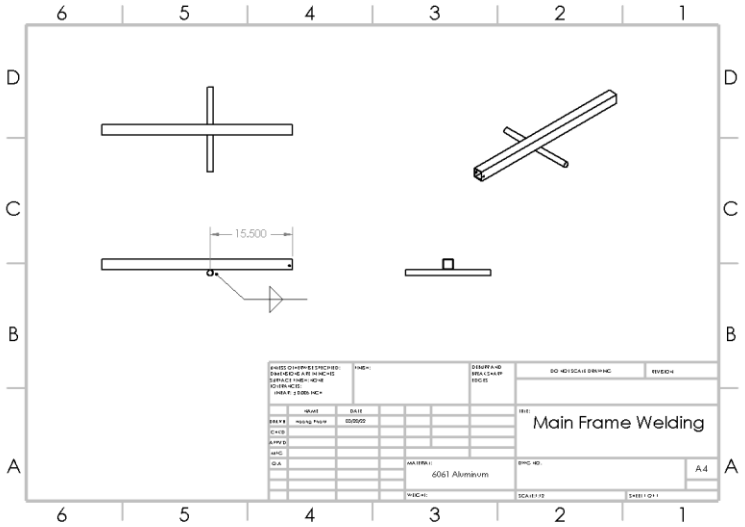
15.500
Main Frame Welding
6061 Aluminum
A4

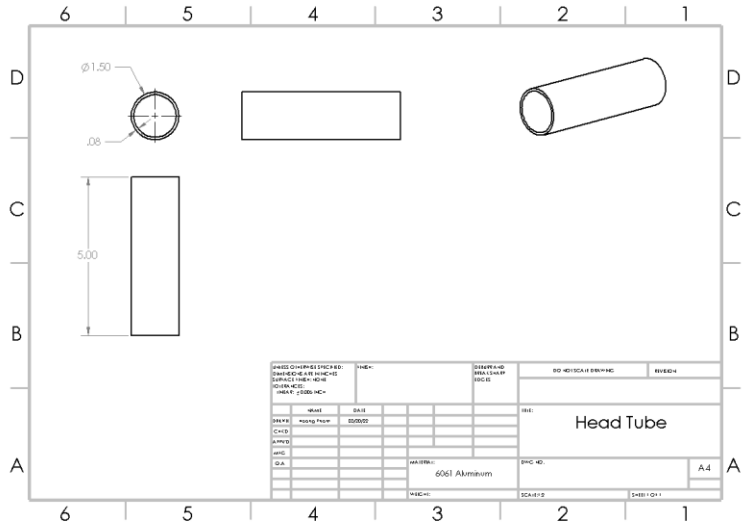
Ø1.50
.08
5.00
Head Tube
6061 Aluminum
A4

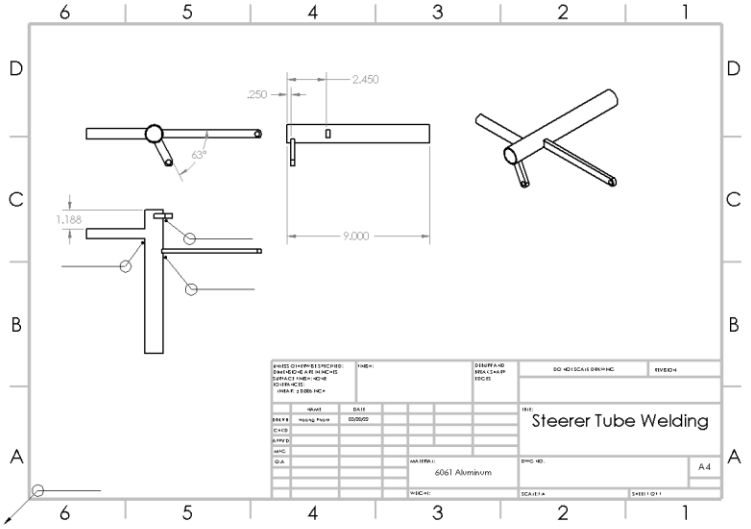
2.450
.250
63°
1.188
9.000
Steerer Tube Welding
6061 Aluminum
A4

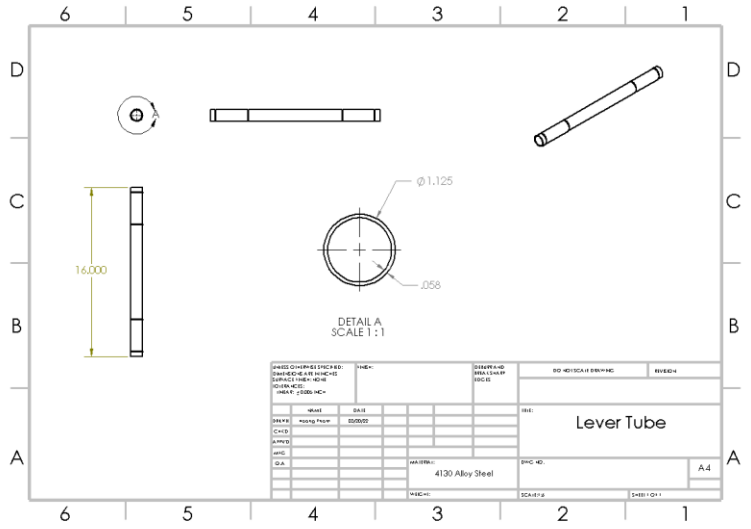
Ø1.125
.058
16.000
DETAIL A
SCALE 1 : 1
Lever Tube
4130 Alloy Steel
A4

Appendix B – Gantt Chart

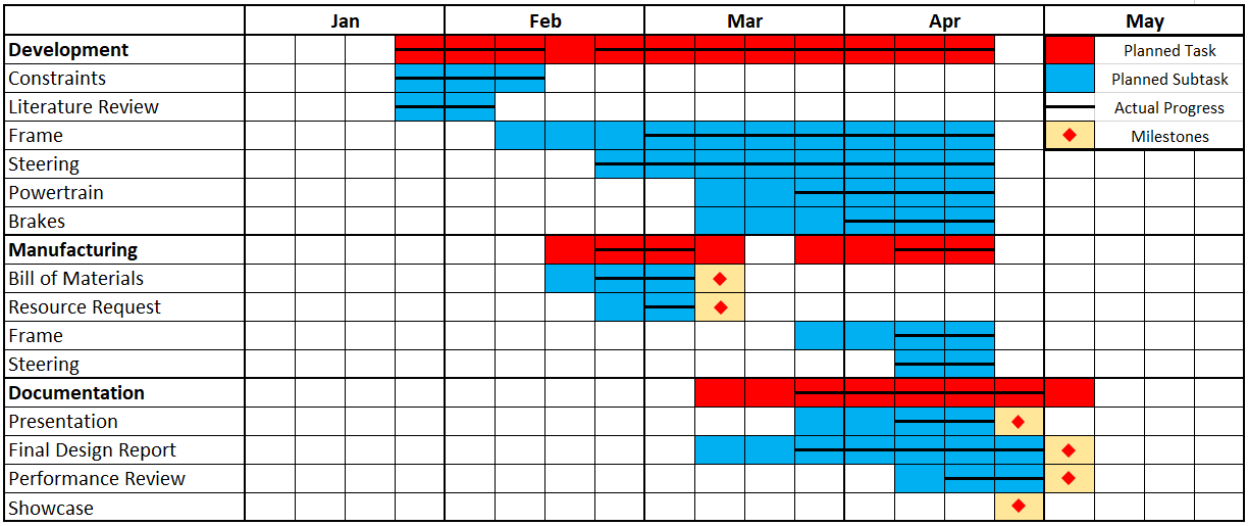

Figure B1: Gantt chart for the project

Appendix C – Programming Codes

Bolts.m – Stress Analysis

```
clc
close all
clear all

%% Vehicle Specification
L = 48; % [in] Wheelbase
b = 26.2; % [in] Front wheel to cg
c = L -b; % [in] Rear wheel to cg

W = 209; % [lb] Weight

% Aluminum
Sy_Al = 40e3; % [psi] Yield strength
E_Al = 10e6; % [psi] Young's modulus

%% Bolt Speciification (Front)

% Grade 8 steel
Sp = 120e3; % [psi] Proof strength
St = 150e3; % [psi] Tensile Stength
Sy = 130e3; % [psi] Yield Strength
E = 29e6; % [psi] Young's modulus

% Geometry
db = 0.25;
A = 1/4*pi*(db)^2;
At = 0.0269; % [in^2] Minor diameter area

%% Bolts configuration

d = 14.76; % [in] Front wheel to centroid of bolts
theta = 14.6; % [deg]

bs = 0.75; % [in] Bolt spacing
r1 = 1.5*bs;
r2 = bs/2;
r3 = r2;
r4 = r1;
%% Wheel load

Wf = c/L*W;
Wr = b/L*W;

%% Force calculation
% Moment about the centroin of the bolts
M = Wf*d;

% Primary shear force
f1 = Wf/4;

% Secondary shear force
s = r1^2 + r2^2 + r3^2 + r4^2;

f2 = M*r1/s;

%% Total shear force

f = sqrt(f1^2 + f2^2 + 2*f1*f2*cosd(theta));

%% Stress calculation

% Shear stress
tau = f/At; % Threaded area

% Factor of safety
```

```
ny = Sy/tau;

%% Bearing stress
t = 0.125; % [in] Frame thickness

sigmab = f/(6*t*db);

ny_b = Sy_Al/sigmab;

%% Bending stress

dmax = 15.85; % [in] Front to farthest bolt

Mmax = Wf*dmax;

bf = 2; % [in] Base of frame
hf = 2; % [in] Height of frame

bi = bf - 2*t;
hi = hf - 2*t;

d2b = 0.25; % Distance from neutral axis to bolt center

I = 1/12*bf*hf^3 - 1/12*bi*hi^3 - 2*(1/12*t*db^3 + t*db*d2b^2);

sigma_edge = Mmax*bf/2/I;

ny_edge = Sy_Al/sigma_edge;

Kt = 3; % Stress concentration
sigma_fbolt = Kt*Mmax*(d2b+db/2)/I; % Stress of frame at bolt edge

ny_fbolt = Sy_Al/sigma_fbolt;

%% For the smaller bar
bf2 = 1;
hf2 = 1;

bi2 = bf2 - 2*t;
hi2 = hf2 - 2*t;

I2 = 1/12*bf2*hf2^3 - 1/12*bi2*hi2^3 - 2*(1/12*t*db^3);
sigma_edge2 = Mmax*hf2/2/I2;

ny_edge2 = Sy_Al/sigma_edge2;

sigma_fbolt2 = Kt*Mmax*(db/2)/I2;

ny_fbolt2 = Sy_Al/sigma_fbolt2;

%% Rear bolts specification (Tension)

dbr = 5/16; % [in] diameter
Abr = 1/4*pi*(dbr)^2; % [in^2] Non-threaded cross-section
Atr = 0.0524; % [in^2] Threaded cross-section
ldbr = 0.625; % [in] Non-threaded length
ltr = 0.875; % [in] Threaded length

%% Rear bolt stiffness

kb = (Abr*Atr*E)/(Abr*ltr + Atr*ldbr);

%% Member Stiffness

dhole = 5/16;
t1 = 0.065;
t2 = 0.065;
t3 = 0.05;

D1 = dhole*1.5;
k1 = stiff(E_Al,D1,dhole,t1);
```

```
D2 = D1 + 2*t3*tand(30);
k2 = stiff(E_Al,D2,dhole,t2);

D3 = D1;
k3 = stiff(E,D3,dhole,t3);

km = 1/(1/k1 + 1/k2 + 1/k3);

%% Bolt stresses

C = kb/(kb+km); % Joint stiffness constant

fi = 0.75*Atr*Sp; % Preload

P = Wr/2; % Force at the joint

np_rbolt = Sp*Atr/(C*P + fi); % FOS for proof strength

nl_rbolr = (Sp*Atr - fi)/(C*P); % Load factor

n0 = fi/(P*(1-C)); % FOS for joint seperation

%% Rear bolt in shear

% Streses
tau_rb = P/Atr;

ny_rb = Sy/tau_rb;

%% Print results (FOS)
fprintf('FOS for the shear of the front bolts: %.2f\n',ny)
fprintf('FOS for the bearing stress of frame: %.2f\n',ny_b)
fprintf('FOS for the bending of the large bar at the edge: %.2f\n',ny_edge)
fprintf('FOS for the bending at the edge of the bolt (large bar): %.2f\n',ny_fbolt)
fprintf('FOS for the bending of the small bar at the edge: %.2f\n',ny_edge2)
fprintf('FOS for the bending at the edge of the bolt (small bar): %.2f\n',ny_fbolt2)
fprintf('FOS for the tension rear bolt (proof): %.2f\n',np_rbolt)
fprintf('FOS for the joint seperation rear bolt: %.2f\n',n0)
fprintf('Load factor for the rear bolt: %.2f\n',nl_rbolr)
fprintf('FOS for the shear of the rear bolts: %.2f\n',ny_rb)

%% Function
function k = stiff(E,D,d,t)
    k = (0.5774)*pi*E*d/(log(((1.155*t+D-d)*(D+d))/((1.155*t+D+d)*(D-d))));
end
```

optimization1.m – Steering mechanism optimization (Use jointly with ackerman3.m)

```
close all
clear all

%% Inputs
L = 4; % Wheelbase [ft] 5 3.83
T = 2.83; % Kinematic track [ft] 2.08
R_min = 26.2; % Min turn radius [ft]

x0 = [4/12 60 L T R_min]; % Starting point
ackerman3(x0);

%% Optimize using fminunc
% options = optimoptions('fminunc','Display','iter');
% [x,fval] = fminunc('ackerman2',x0,options);
% x
% fval

%% Optimization using fmincon
A = [];
b = [];
Aeq = [];
beq = [];
nonlcon = [];

lb = [2/12 0 L T R_min]';
ub = [2/12 90 L T R_min]';

options = optimoptions('fmincon','Display','iter','PlotFcn','optimplotfval');
[x,fval] = fmincon('ackerman3',x0,A,b,Aeq,beq,lb,ub,nonlcon,options);
grid on
ylabel('MSE')

%% Calculate track rod length
l = T - 2*x(1)*cosd(x(2));

%% Print results
fprintf('\n')
fprintf('Track rod length: %.4f ft\n',l)
fprintf('Steering arm: %.4f ft\n',x(1))
fprintf('Neutral angle: %.4f ft\n',x(2))
fprintf('Mean square error: %d\n',fval)
```

ackerman3.m

```
function mse = ackerman3(x)
%% Givens
L = x(3); % Wheelbase 6.5 [ft]
T = x(4); % Kinematic track 2.5 [ft]
R_min = x(5); % Min turn radius 26.2 [ft]
R = linspace(R_min,500,5000)';

%% Inputs
l = x(1); % Steering arm
theta0 = x(2); % Neutral angle
% theta0 = 71;

%% Theoretical Ackerman Angles
del_i = atand(L./(R-T/2));
del_o = atand(L./(R+T/2));

%% Calculate steering linkage lengths
a = l;
b = T - 2*l*cosd(theta0);
c = l;
d = T;
```

```
%% Linkage Position Analysis
% Calculate angles from min radius to neutral steer
theta_test = theta0 + del_o; % Prescired outer steer angle

theta3 = zeros(length(theta_test),1);
theta4 = zeros(length(theta_test),1);

for i = 1:length(theta_test)
    theta2 = theta_test(i);
    %% Coefficients
    k1 = d/a;
    k2 = d/c;
    k3 = (a^2 - b^2 + c^2 + d^2)/2/a/c;
    k4 = d/b;
    k5 = -(a^2 + b^2 - c^2 + d^2)/2/a/b;

    %% Intermediate Coefficients
    A = cosd(theta2) - k1 - k2*cosd(theta2) + k3;
    B = -2*sind(theta2);
    C = k1 - (k2+1)*cosd(theta2) + k3;
    D = cosd(theta2) - k1 + k4*cosd(theta2) + k5;
    E = -2*sind(theta2);
    F = k1 + (k4-1)*cosd(theta2) + k5;

    %% Calculate theta3 and theta4
    theta3 = 2*atand((-E - sqrt(E^2-4*D*F))/2/D);

    theta4(i) = 2*atand((-B - sqrt(B^2-4*A*C))/2/A);
end

%% Calculate mean square error
% Calculate actual inner steer angle
del_i_actual = theta4 - (180-theta0);

% Compare with ideal ackerman inner angle
error = del_i_actual - del_i;

% Calculate mean square error
mse = norm(error)/length(error);

end
```

SteeringSensitivity.m – Steering control analysis

```
close all
clear all

%% Givens
% Coordinates of the center of the steerer tube bracket
x0 = 5.5; % 7, 5.5
y0 = 15; % 21.5
z0 = -0.5; % -0.5
% l = 22.5; % 23

% Max rotation angle for the steerer tube bracket
dtheta_max = 15;

% Initial angle of the lever [bracket hole] from the vertical axis
theta0 = 20;
%%
R1 = 3; % 4; lever length
R2 = 6.5; % 8.5; steer tube bracket length

theta_test = 90 - theta0; % Initial angle from the horizontal axis

% l = sqrt((x0 - R2)^2 + y0^2 + (z0 - R1)^2);

% Calculate the coupler length
l = sqrt((x0 - R2)^2 + (y0 - R1*cosd(theta_test))^2 ...
```

```
    + (z0 - R1*sind(theta_test))^2);

%% Calculate the angle
% Prescribe the test angles for the steer tube bracket
t2_test = linspace(0,15,50);

% Gif paramters
fr = cell(length(t2_test),1); % frames
ft = 0.05; % time between frames

for i = 1:length(t2_test)
    t2 = t2_test(i);

    %% Solve for the lever horizontal angle

    f = @(t1) [(x0 - R2*cosd(t2))^2 ...
               + (y0 + R2*sind(t2)- R1*cosd(t1))^2 ...
               + (z0 - R1*sind(t1))^2 - l^2];

    t0 = 1;

    t = fsolve(f,t0);
    t_test = 90 - t; % Vertical level angle
    del_t = t_test - theta0; % Calculate the change in angle
    f(t);

    %% Plot the results

    x = [0 0 x0-R2*cosd(t2) x0]';
    y = [0 R1*cosd(t) y0 + R2*sind(t2) y0]';
    z = [0 R1*sind(t) z0 z0]';

    plot3(x,y,z,'o-')
    grid on
    axis equal
    view([62.9674 37.8654])
    ylim([0 17])
    zlim([-0.5 3])
    set(gca,'box','off','xcolor','none','ycolor','none','ZColor','none')
    set(gcf,'Color','white')
    fr{i} = frame2im(getframe(gcf));
%     pause(0.05)
end
%%
sensitivity = dtheta_max/del_t

%% Output image

filename = 'Control.gif';
for iii = 1:length(t2_test)
   [A1,map] = rgb2ind(fr{iii},256);
   if iii == 1
        imwrite(A1,map,filename,'gif','LoopCount',Inf,'DelayTime',ft);
   else
        imwrite(A1,map,filename,'gif','WriteMode','append','DelayTime',ft);
   end
end
```

Drivetrain.m – Drivetrain analysis

```
% Capstone Gearing simulation

Crankset = [34; 50];
Casette = [11 13 15 18 21 24 30 37 46];
Ratios = Casette./Crankset
Cadence = 75; %rpm
WheelRPM = Cadence./Ratios;
WheelD = 20; %inch
%Assuming no friction loss
```

```
Speed = WheelRPM*WheelD*pi; %in/s
SpeedMPH = Speed*60/63360 %MPH
```

Brakes.m – Calculate stop time

```
close all
clear all

%% Givens
v = 22.78; % [ft/s] intial velocity
v0 = 0; % [ft/s] final velocity
s = 19.7; % [ft] distance

d = 22/12; % [ft] wheel diamter
m = 4/32.2; % [slugs] wheel mass
r = d/2; % [ft] wheel radius

I = m*r^2; % [slug.ft^2] wheel moment of inertia
%% Acceleration
a = (v^2-v0^2)/2/s; % [ft/s^2] deceleration
alpha = a/r; % [rad/s^2] angular deceleration
%%  Torque

T = I*alpha; % [lb.ft] Torque required for braking

%%
w = 22.78/(10/12); % [rad/s] inittial angular velocity

tf = w/(T/I); % [s] total time to stop

%% Plot results
t = linspace(0,tf,50);

w1  = w - t*T/I; % [rad/s] angular velocity over time

plot(t,w1)
xlabel('Time [s]')
ylabel('Angular Velocity [rad/s]')
grid on

%% Brake pad pressure
m = 209/32.2; % [slugs]

mu = 0.4; % friction coefficient
BrakePadArea = 0.6; % [in^2]
r_brake = 0.32; % [ft]

Fb = (m*(v^2-v0^2)/2)/s; % [lb] Based on energy theory

F_applied = Fb*r/mu/r_brake; % [lb]

Pressure = F_applied/BrakePadArea; % [psi]

%% Print Results

fprintf('The pressure at brake pad: %.1f psi\n',Pressure)
```

Appendix D – Full Spreadsheets used for calculations, data, project tracking

Sample calculation for the factor of safety:

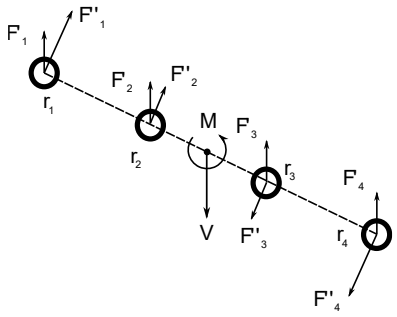

Figure D1: FBD for the bolts

The shear force will equal to the front wheel load as:

$$V = W_f = \frac{21.8\ in}{48\ in} 209\ lb = 95\ lb$$

Therefore, the primary shear for the first bolt will be:

$$F'_1 = \frac{V}{4} = \frac{95\ lb}{4} = 23.8\ lb$$

The moment at the centroid of the bolts is:

$$M = W_f d = 95\ lb \times 14.7\ in = 1401\ lb.in$$

As a result, the secondary shear at the first bolt will be:

$$F''_1 = \frac{Mr_1}{r_1^2 + r_2^2 + r_3^2 + r_4^2} = \frac{1401(1.12)}{1.12^2 + 0.375^2 + 0.375^2 + 1.12^2} = 560\ lb$$

Therefore, the total force acting on the first bolt will be:

$$F^2 = (F'_1)^2 + (F''_1)^2 + 2(F'_1)(F''_1)\cos(\theta) = 23.8^2 + 560^2 + 2(23.8)(560)\cos(14.6°)$$

$$F = 583\ lb$$

The bolt has a major diameter of 0.25 in, and the threaded area is in contact with the frame. The max shear stress will occur over the threaded area.

$$\tau = \frac{F}{A_t} = \frac{583\ lb}{0.0269\ in^2} = 21.7\ ksi$$

Therefore, the factor of safety of the bolt (grade 8 steel) in shear will be:

$$n_Y = \frac{S_y}{\tau} = \frac{130\ ksi}{21.7\ ksi} = 5.99$$

The factor of safety of remaining bolts are calculated similarly.

Appendix E – Copies of the ME Departmental Supply and Resource Request Forms

University of Massachusetts Lowell

Department of Mechanical Engineering

One University Avenue

Lowell, Massachusetts 01854

Capstone Resource Form

To be completed by Requester

Student Name(s): Hoang Pham, Steven Beaupre, Derek Chigas, Michael Mears

Course Section: 804

Capstone Instructor: Abouhamed Saberi

Capstone Project ID: ME-S22-23

Date: 3/21/2022

Description of Resource(s)/Service(s):

Attach all drawings for machining/fabrication, electrical schematics for electronic fabrication, testing standards and test matrix. Include details about what you will be doing under supervision and what you need to have performed by department staff. Include number of parts or samples.

Drilling:

The Makerspace will be needed to drill holes in sheet metal and rectangular tubes.

A drill press would also be requested for higher precision.

Areas that need drilling:

- Mounting holes for the main frame
- Mounting holes for the rear frame
- Holes for the brackets

Cutting:

The Makerspace will be needed to cut square steel tubing, both complete through cuts and round cuts to mate to circular tubing. Circular tubing will be cut into parts.

The CNC machines will be requested to cut sheet metal into brackets (May require department staff assistance).

Parts that need cutting:

- Rear frame
- Head tubes
- Steerer tube
- Wheel tube
- Lever
- Lever tube
- Steering linkage (from threaded rods)
- Bracket to connect linkages (from sheet metal)

Machining:
A lathe will be requested to make grooves on a round tube for retaining rings.

Areas that need machining:

- Round tube for the lever tube mount

Welding:

Welding will be needed to attach rectangular and circular steel tubes. It will also be used to attach brackets to circular steel tubes. We talked to the president of the Formula Student team and can partner with them and their welder to weld these parts.

Areas that need welding:

- Head tubes to the rear frame
- Round tube to the main frame
- Lever and bracket to the lever tube
- Wheel tube and brackets to the steerer tube

All drawings for machining/fabrication are included in the attached zip file.

To be completed by Department Staff

Resource Hours Required:

Approximate Dates/Times:

Department Staff Signature: _____ Date: _____

To be completed by Capstone Instructor

I certify that the capstone project, including this form and associated attachments, has satisfactorily completed the design review and is approved to use/arrange the described resources.

Capstone Instructor Signature: *Abouhamed Saberi* **Date: 03/21/2022_____**

Capstone student(s) should submit this form to the department staff to schedule the resources or services only after signed by both the Department Staff and Capstone Instructor. Students should retain a copy of this form to include in Capstone Final Report.

This completed form must be received by March 18, 2022 to request departmental resources.